NOTE TO USERS

This reproduction is the best copy available.

A LOCAL-FEEDBACK-GLOBAL-CASCADE MODEL FOR HIERARCHICAL HEART RATE VARIABILITY IN HEALTHY HUMANS

by

Xiuzhong Gao

BEng. Mechanical Engineering

Dalian University of Technology, China 1984

A Thesis

presented to Ryerson University

in partial fulfillment of the

requirements for the degree of

Master of Applied Science

in the program of

Mechanical Engineering

Toronto, Ontario, Canada 2004

BORROWER'S PAGE

Ryerson University requires for the signature of all persons using or photocopying this thesis.

Please sign below and give address and date.

A Local-Feedback-Global-Cascade Model For Hierarchical Heart Rate Variability In Healthy Humans

Xiuzhong Gao, Master of Applied Science in the program of Mechanical Engineering, Ryerson University 2004

ABSTRACT

A broad view on Heart Rate Variability (HRV) study is made and the hierarchical structure is shown in Local-feedback-Global-Cascade (LFGC) model, which is built to explore the role of reflex feedback. This feedback, which integrates additive and multiple functionalities in multifractal cascade models, functions on the She-Waymire (SW) form of the hierarchical structure so that the concept of defect dynamics can be applied to LFGC model. The experimental evidence verified the existence of the hierarchical structure and showed discrete scale invariance in data supported the additive feedback law, which may exist in the cardiovascular system in harmony with this dynamical cascade model.

ACKNOWLEDGEMENT

I would like to thank my supervisor Dr. Der Chyan Lin for his encouragement and help with this thesis. With his great patience Professor Lin guides me into this new field- time series analysis in physiological systems. I appreciate his support and scrutiny with the work I have done and thank him for keeping me spirits up and encouraging me to explore things new. All of these will help me a lot in the future. I also would like to thank Ryerson' all faculty and staff for giving me support during my study.

Table of Contents

List of Figures

List of Tables

Nomenclature

Mathematical Symbols

$\sim$	Proportional to
$\underline{\underline{d}}$	Equal in distribution
$\langle \bullet \rangle$	Statistical average

Latin Symbols

A_p	A function of p
B_j	Averge absolute difference between weights and reference set points
C	Parameter of the hierarchy
$d_k^{(j)}$	Update interval for the jth generation cascade component
f_0	Arbitrary factor
h_0	Parameter of the hierarchy
G	Power spectral density
H	Hurst exponent
j	Cascade generation index
J	Total number of cascade generations
K	Kurtosis
$K(\tau)$	Kurtosis as a function of time scale

l	Spatial scale
l_0	Special spatial scale
$r(t)$	RRi between t th and $(t+1)$ th heart beats
$r_J(t)$	Simulated RRi time series
$S_p(l)$	pth order structure function in spatial scale
$S_p(\tau)$	pth order structure function in temporal scale
t	Integer time
$t_k^{(j)}$	Update time for the cascade component
V_j	Control set point in jth cascade generation
$v(l)$	Velocity function
w	Gaussian Variable of mean 0 and standard deviation 1
Y	Poisson variable

Greek Symbols

α	Cascade model parameter
β	Hierarchy exponent
β^γ	Modulating component of the SW cascade
γ	Kurtosis exponent
$\delta_j = 2^{(J-j)}$	Update interval for the jth generation dyadic cascade component
$\delta^{(J)}$	Cascade parameter
$\Delta v(l)$	Velocity increment
$\Delta r(\tau)$	RRi increment function

$\Delta r_j(\tau)$	Simulated RRi increment function
$\zeta(p)$	Structure function exponent
λ	Density of the Poisson distribution in SW cascade.
μ_j	Mean value of the *j*th cascade component
ρ	1/f – power law exponent
τ	Increment time or time scale
σ_j	Standard deviation of the *j*th cascade component
σ_0	Constant
χ	$(l/l_n)^{\gamma}$
$\omega_j(t)$	Cascade component
ω_m	Cascade component of the *m*th generation in SW cascade

Chapter1

Introduction

1.1 Introduction of Cardiovascular Regulation

The study of cardiovascular regulation consists of at least two major subfields: the heart and its peripheral organs and the dynamics and control of the heart rate. The former subject concerns mainly the mechanics of the heart, the vascular systems and the lung. The latter subject concerns the interaction between the autonomic nervous system with the heart, the vascular and respiratory systems as well as their integration in the higher control centers in the brain stem. Hence, the heart rate fluctuation describes one of the most complex phenomena in nature. In particular, it characterizes the system behavior of the whole body and cannot be related to just one single set of organ functionalities. Given the vast body of literature on this subject, the scope of this introduction will be focused on the basic elements in the regulation of the heart rate.

The main objectives of cardiovascular regulation are to provide rapid transport of oxygen and nutrients, as well as to take away heat and metabolic wastes around the body. It relies on many "sensors" and "actuators" distributed in the body to achieve coordination of heart rate, blood circulation and respiration in order to perform the complicated task of cardiovascular regulation. The sensor inputs, or more commonly known as the afferent

inputs, are derived from the so-called receptor sites in various locations of the body. They eventually converge at the spinal cord and then travel to the cardiovascular centers at the brain stem. After processing such signals via still largely unknown mechanisms, outputs or the efferent signals will arrive at the "actuator" sites in the lung, vascular system and the heart to perform normal functions of these organs.

At the level of the heart, the efferent signal reaches the heart at the primary pacemaker site known as the sino-atrial (SA) node. The sequence of events following the excitation of the SA node can be summarized in four stages (Figure 1): the contraction of the atria, excitation of the atrial-ventricular node located at the wall between atria and ventricles, excitation of the Perkinje fibers, and the contraction of the ventricles. The occurrence of these events can be measured from the (small) potential difference on the surface of the chest. This type of measurement is used to produce what is called the electrocardiogram (ECG). The contraction of the ventricles introduces a sharp peak in the ECG time trace and its location is designated as the R wave. The time span between the R waves, known as the RR interval (RRi), is precisely the inverse of the heart rate (See Figure 1). Mainly due to it easy access, RRi has been used as the primary variable for analysis in Heart Rate Variability.

The messenger system that is responsible for delivering sensor and actuator signals is the highly convoluted autonomic nervous system. When minor disturbance from either an internal or external source is present, the vascular system may regulate the blood circulation via muscle constriction or dilation. When a disturbance persists and reaches a

significant level, the regulation must be accompanied by a system response such as increasing or decreasing the heart rate.

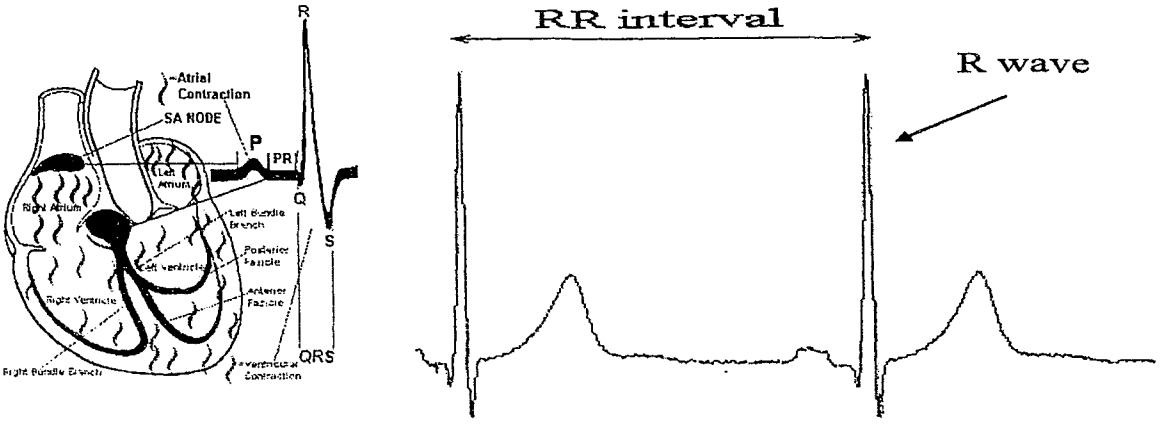

Figure 1. (a) Heart and R wave. (b) RR interval (RRi).

Although using RRi to assess cardiovascular health is desirable since it is noninvasive, it captures nothing but the overall behavior of the cardiovascular dynamical system. It thus represents one of the most complex signals known in nature. It is known that a healthy cardiovascular system manifests itself in violent fluctuation of RRi. Counterintuitive to the conventional belief, heart disease is normally associated with significantly lower RRi variability. The purpose and the origin of heart rate fluctuation remain largely unknown to-date, and they continue to be the subject of interest for clinicians, physiologists, physicists and mathematicians.

1.2 Heart Rate Variability and Characteristics of Ambulatory RR Intervals

Heart rate variability (HRV) is the term used to describe the apparent random fluctuation of RRi on a beat-to-beat basis. From the autonomic regulation point of view, HRV is a result of the intricate balance between the sympathetic (SNS) and parasympathetic nervous systems (PNS), where SNS tends to accelerate the heart rate (shorten RRi) and PNS tends to decelerate the heart rate (lengthen RRi). Although little is known regarding its physiological background, clinical data already show that HRV can provide an indirect measure of the health of the cardiovascular system since the mortality rate of heart diseased patients has been found to be inversely proportional to the degree of HRV. This section will demonstrate the characterization of RRi fluctuation. Following the language in statistical physics, this characterization is called *HRV phenomenology*.

Throughout the entire thesis, $r(t)$ will be used to denote the RRi between the t th and $(t+1)$ th heart beats and the RRi increment defined at a given time scale τ is given by:

$$\Delta r(\tau) = r(t+\tau) - r(t) \tag{1}$$

A. 1/f Power Spectrum

Given the $r(t)$, the power spectral density function, $G(f)$, can be calculated using discrete-time fast Fourier transform (DFT):

$$X(\omega)=\sum_{t=-\infty}^{+\infty} r(t)e^{-j\omega t}$$

where ω is the frequency, $j=\sqrt{-1}$. Numerically, the time series is divided into overlapping sections, each of which is first detrended, and then Hanning windowed. The magnitude squared of the DFT of the sections are finally averaged to give $G(f)$ up to the Nyquist frequency $\omega = 0.5$.

Kobayoshi and Musha [1] reported the earliest result of power law in HRV. They found the power spectrum of $r(t)$ has the following form

$$G \sim f^{-\rho} \tag{2}$$

where G is the power spectral density, f is the frequency in either Hz or 1/beat, and $\rho > 0$ is the power law exponent. For healthy subjects, ρ was found to be ≈ 1. In general, ρ can vary with physiological or pathological conditions [2, 3]. In particular, ρ in heart disease is typically larger. In a clinical setting, this finding was used to suggest an inverse relationship between the degree of HRV and the health of the cardiovascular system. The RRi power spectrum from the daytime, ambulatory, RRi recording of a healthy subject is plotted in Figure 1[1]. The 1/f-like power law is evident.

[1] The database used in this section is described in section 2.2.

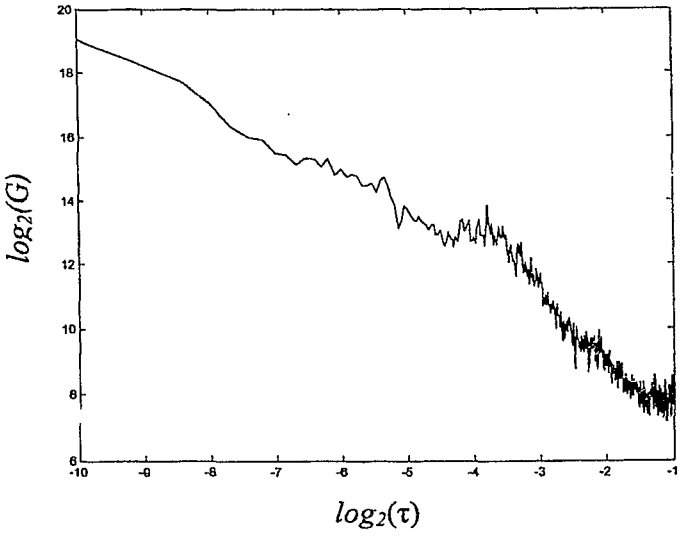

Figure 2. Power law power spectrum from healthy daytime HRV.

B. Self-similar Fluctuation of RRi

The 1/f-like power spectrum is known as the necessary condition for the property called self-similarity or scale invariance. A self-similar process is also called a fractal process. This property implies long-time memory or correlation in the underlying cardiac control process and supports the view that HRV is temporally *fractal* [4].

Mathematically, the notion of a self-similar process $x(t)$ can be formulated as

$$x(\lambda t) \underline{\underline{d}} \lambda^H x(t) \tag{3}$$

where λ are an arbitrary constant, H, a parameter known as the Hurst exponent and $\underline{\underline{d}}$ means "equal-in-distribution." This definition means "patterns" repeat themselves over a magnification of scale by a λ factor. The same RRi data that was used to generate the

power spectrum in Figure 2 is plotted in Figure 3. It is possible to qualitatively find the self-similarity of this time series. For example, Figure 4 plotted the same time series over $17600 \leq t \leq 18300$. It is seen that similar patterns exist in Figures 3 and 4. This is the demonstration of self-similarity in HRV. It should be noted quantitative verification of self-similarity cannot be achieved by (3) since it is not possible to find the exact distribution from numerical data. Generally, one may rely on the statistics derived from the distribution. For example, the power spectrum, which characterizes the second order statistics of the distribution, is a necessary condition for self-similarity.

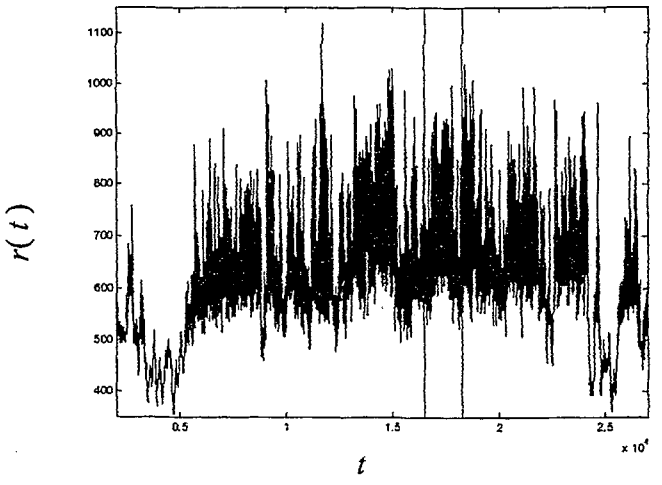

Figure 3. RRi data for a typical healthy subject.

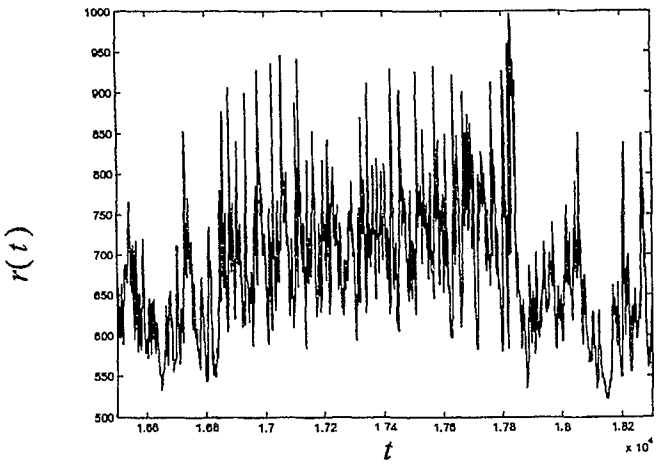

Figure 4. A segment from figure2 (between vertical lines).

C. Increment Probability Density Function (PDF)

It was found that the increment probability density function (PDF) of healthy RRi typically shows the stretch-exponential → exponential → Gaussian (SEG) transition as the time τ increases [5]. The same data in previous Figures is used to calculate normalized histograms of $\Delta r(\tau)$ for $\tau = 2^0, 2^4, 2^8, 2^{11}$. The results are used to approximate the increment PDF plotted in Figure 5. The SEG transition is evident.

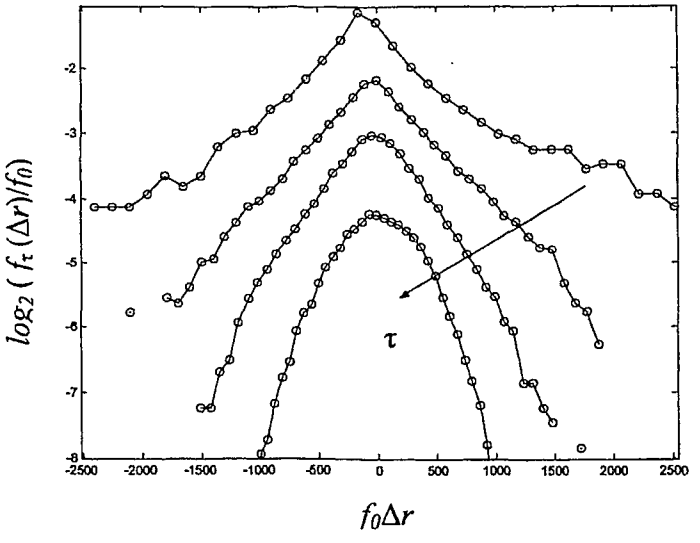

Figure 5. The increment PDF $f_\tau(\Delta r)$ for a typical RRi data set for $\tau = 2^0, 2^4, 2^8, 2^{11}$ (increasing in arrow direction). All curves are rescaled horizontally and vertically by arbitrary factors f_0 and $1/f_0$, respectively, for clarity purpose.

The SEG transition has also been found in the PDF of the velocity increment. It has been successfully demonstrated in some turbulence models [6] and time series models constructed by summing Gaussian variables on the dyadic tree [7].

The transition may be characterized quantitatively by using conventional statistics. In what follows, the kurtosis of the increment PDF will be used to characterize the SEG transition.

The kurtosis K is defined as the normalized fourth order central moment: given any random variable X with mean μ and variance σ^2

$$K = \frac{\langle (x-\mu)^4 \rangle}{\sigma^4} \approx \frac{\sum (x-\mu)^4}{N\sigma^4} \tag{4}$$

where N is the number of samples [8]. Although kurtosis has been a classical statistic, there is in fact no agreement as to what it can specifically characterize [9]. Some reseachers show that kurtosis captures the peakedness and flatness of the PDF and others emphasize the dependence of kurtosis on the tail behaviour [10, 11].

For the purpose of this work, the K value of the increment PDF is used to compare the theoretical values in the SEG transition. Specifically, the kurtosis for normal distribution has a value $K = 3$. A larger $K > 3$ results for distributions which are more outlier-prone than the normal distribution. In particular, the kurtosis of the exponential distribution is

$K = 9$. A smaller $K < 3$ results for distributions which are less outlier-prone than the normal distribution.

The K value was estimated for $\Delta r(\tau)$ at $\tau = 2^0 ... 2^{14}$ and their values are plotted in Figure 6 in logarithmic scales.

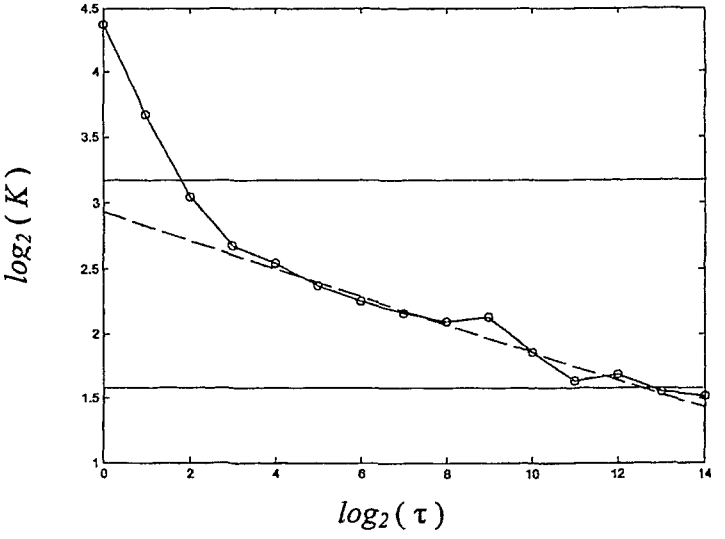

Figure 6. The Kurtosis curve estimated from the increment PDF of a typical RRi data set. The theoretical values for exponential & Gaussian K's are shown as horizontal lines at $\log_2(9)=3.1699$ and $\log_2(3) = 1.5850$, respectively.

The range of values covered by K is clearly compatible to the view of SEG transition suggested by Figure 5. Furthermore, the existence of a power law relationship was found:

$$K(\tau) \sim \tau^{\gamma}. \tag{5}$$

This power law relationship can be explained by the empirical law:

$$S_p(\tau) = \left\langle |\Delta r(\tau)|^p \right\rangle \sim \tau^{\zeta(p)} \tag{6}$$

where $\langle \bullet \rangle$ denotes statistical average and $p > 0$ is a real number. Equation (6) can be applied in (4) by letting $x = \Delta r(\tau)$. Since $\mu = \langle \Delta r(\tau) \rangle = 0$, the kurtosis becomes

$$K = \frac{\langle \Delta r_J(\tau)^4 \rangle}{(\sigma^2)^2} \sim \frac{\tau^{\zeta(4)}}{\tau^{2\zeta(2)}} = \tau^{\zeta(4)-2\zeta(2)} \tag{7}$$

Hence, $\gamma = \zeta(4) - 2\zeta(2)$. More details about the empirical law (6) are discussed next.

D. Multifractal HRV

The empirical law (6) describes a power law structure function in HRV. This can be observed in Figure 7 where $S_{1.2}(\tau)$ of the data used previously is plotted against τ in log-log scales. Such a power law is in fact consistent with the definition of a scale invariant process (3). However, (3) cannot predict the property of the scaling exponent $\zeta(p)$. By varying p = 0.25, 0.5, ..., 5, $\zeta(p)$ can be estimated numerically and is shown in Figure 8. It is seen that $\zeta(p)$ is nonlinear. This is a typical property for HRV [5]. In the literature, a fractal process showing linear $\zeta(p)$ is said to exhibit monofractal scaling. In contrast, a nonlinear $\zeta(p)$ implies multifractal scaling [5]. The notion of multifractality has been established in the frameworks of martingale theory of stochastic processes and large deviation theory in probability theory. It is beyond the scope of this thesis to conduct the analysis following such rigors. To study and investigate the change of the scaling property in HRV, $\zeta(p)$ will be used as a working definition to distinguish multi– (a nonlinear $\zeta(p)$) and monofractality (a linear $\zeta(p)$).

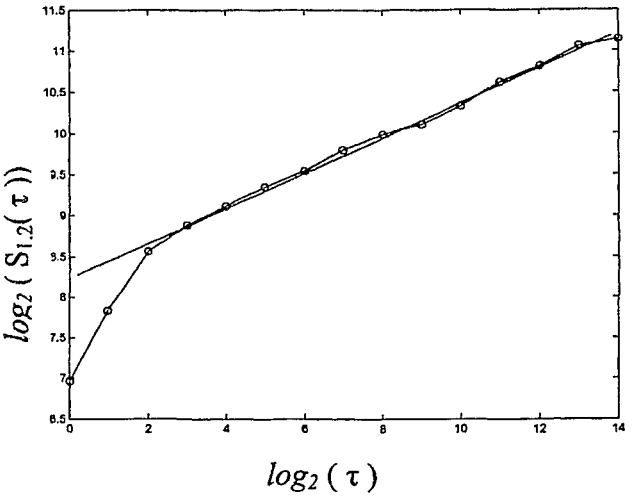

Figure 7. The power law $S_p(\tau)$. The straight line demonstrates the linear fit of the power law.

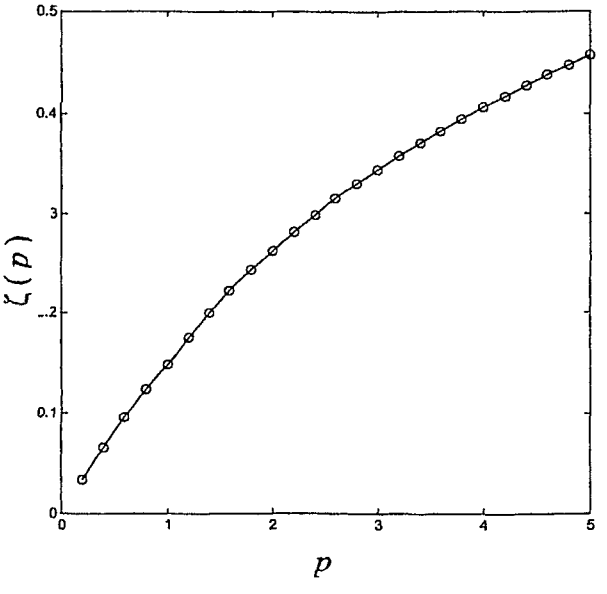

Figure 8. $\zeta(p)$ curve for the data shown in Figure 6.

1.3 Heart Rate Variability as a Complex Dynamics Problem: Turbulence Analogy and Phenomenological Models

It was found that the HRV phenomenology is in many ways compatible to those observed in fluid turbulence. For example, both systems exhibit power law, SEG transition of the increment PDF and multifractal scaling. This has been known as the turbulence analogy of long-term HRV [12]. Following this analogy, it was further found that the HRV phenomenology can be effectively captured by using the multiplicative random cascade. The purpose of this section is to review two recent HRV models: the stochastic feedback model (SFM) and the cascade model. These two models provide a sharp contrast in that SFM relies solely on the additive mechanism to generate HRV, whereas cascade relies on the multiplicative mechanism. Both models provide the reference for the new model proposed in this work.

1.3.1 Stochastic Feedback Model

SFM was introduced by P.C. Ivanov et al. to simulate the 1/f-like power law spectrum in HRV [13]. It was the first model that contains elements related to the physiology of the cardiovascular system. This particular aspect provides the main contrast to the entire phenomenology–based cascade model introduced in the next. Although SFM contains certain physiology elements, it missed the very basic component of multiplicative mechanism or cascade in HRV.

The SFM assumes a time-dependent "equilibrium state" on which the cardiovascular regulation is based. It relies on feedback control to carry out the regulation so that the heart rate can return to the equilibrium state. The quantity that is controlled is exactly the RRi increment $\Delta r(\tau)$ as introduced in Section 1.2. To relate to the physiology, SFM assumes inputs from the SA node activity, I_{SA}, and SNS and PNS activities, I_{SNS} and I_{PNS}, respectively. The RRi increment is determined based on the rule: $\Delta r(\tau) = I_{SA} + I_{SNS} + I_{PNS}$. Hence, the fluctuation is determined entirely by an additive mechanism. Each of the I_{SA}, I_{SNS}, I_{PNS} has its beat-to-beat "equilibrium state" or set-point value denoted as R_{SA}, R_{SNS}, R_{PNS}, respectively. These set-point values are themselves random variables subject to some probability laws and correlation. The physiological activities I_{SA}, I_{SNS}, I_{PNS} are thus "driven" by the fluctuation of the "equilibrium states."

The SFM was found to be very effective in capturing the 1/f-like power law spectrum of RRi. It also predicts some pathologic states by exploring different combinations of the set-point values. However, these "numerical pathologies" are yet to be verified in clinical data.

1.3.2 Multiplicative Random Cascade Model

The cascade model was first proposed by D.C. Lin and R.L. Hughson to capture a broader range of HRV characteristics [5]. The model consists of three elements: the multiplicative data generation, the probability law for the cascade component and the branching rule. Let the cascade RRi between tth and $(t+1)$ th heart beats be $r_j(t)$. The

HRV cascade assumes $r_J(t)$ to be given by the product of J random variables $\{\omega_j(t), j=1,...,J\}$:

$$r_J(t) = \prod_{j=1}^{J} \omega_j(t) \tag{8}$$

The $\omega_j(t)$'s are real-value random processes on discrete times $\{t_k^{(j)} \in \mathbf{N}\}$ where $\omega_j(t) = \omega_j\left(t_k^{(j)}\right)$ for $t_k^{(j)} \le t < t_{k+1}^{(j)}, j = 1, \ldots, J, k = 1, 2, \ldots$. The time sets define the branching structure on which the multiplication is conducted. Let $d_k^{(j)} = t_{k+1}^{(j)} - t_k^{(j)}$ and $\left\langle d_k^{(j)} \right\rangle = \delta^{(j)}$. To ensure a self-similar $r_J(t)$, $\delta^{(j-1)} / \delta^{(j)} = \lambda > 1$ is imposed, where λ is the characteristic scale of the cascade. Since $\lambda > 1$, $\omega_j(t)$ for small j is referred to as the large time scale components, as they fluctuate slowly, and those for large j as the small time scale components, as they fluctuate faster. In this thesis, $\lambda = 2$ is only considered and the resulting cascade is called the *dyadic cascade.*

The simulation conducted in the past assumed that $\omega_j(t) = \mu_j + \mathbf{w}\sigma_j$ where $t \in \{t_k^{(j)}\}$, $\mu_j = 1$, and $\mathbf{w}$ is a Gaussian variable with $\langle \mathbf{w} \rangle = 0$ and $\langle \mathbf{w}^2 \rangle = 1$. Assuming independent $\omega_j(t)$'s helps to simplify the analysis and allows one to write down the analytical form of certain statistics [12,14,15]. Using a different distribution for $\omega_j(t)$ will not change the result presented below. Finally, having σ_j varying with j is motivated from the fact that RRi must be bounded. In addition to the obvious upper bound, RRi is also bounded below since the cardiac cells are refractory: namely, there is a finite time period before the cell membrane can be repolarized to propagate nerve impulses [16]. To ensure a

bounded $r_J(t)$ even in the limit $J \to \infty$, σ_j is assumed to be decreasing in j so $\omega_j(t)$'s for small j are capable of large amplitude fluctuation and those for large j fluctuate mostly around the mean value 1. The implementation of σ_j links the spatial and temporal scales of $r_J(t)$ in a specific way: namely, the large amplitude fluctuation is associated with the large time scale and the small amplitude fluctuation with the small time scale. This spatiotemporal condition further relates the large (small) time scale components to the low (high) frequency content $r_J(t)$. The cascade component with decaying σ_j has been called *bounded cascade* in the literature.

Using $\sigma_j = \sigma_0 2^{-\alpha(j-1)}$ with $\sigma_0 = 2^{-1.5}$, $\alpha = 0.2$ and $J = 15$, the bounded cascade model is able to capture the phenomenology summarized in SEC. 1.2 very well. The simulation result is shown in Figure 9.

1.4 Objectives of Thesis

The main objective of the thesis is to further explore the HRV turbulence analogy by considering the hierarchical structure which was recently discovered in fluid turbulence [17]. The existence of the hierarchy provides an interesting alternative for the cascade construction in HRV. It is of great interest to explore this alternative since the current cascade model contains only a multiplicative mechanism and a biological system is also known to operate via feedback regulation which functions in principle on an addition law. The objective of the thesis is to integrate additive and multiplicative laws to simulate the HRV phenomenology. The hierarchical structure in turbulence provides the first example

to achieve such integration. In particular, evidence for She-Leveque hierarchy in healthy HRV will be presented and the known hierarchy solution will be modified to build the new HRV model.

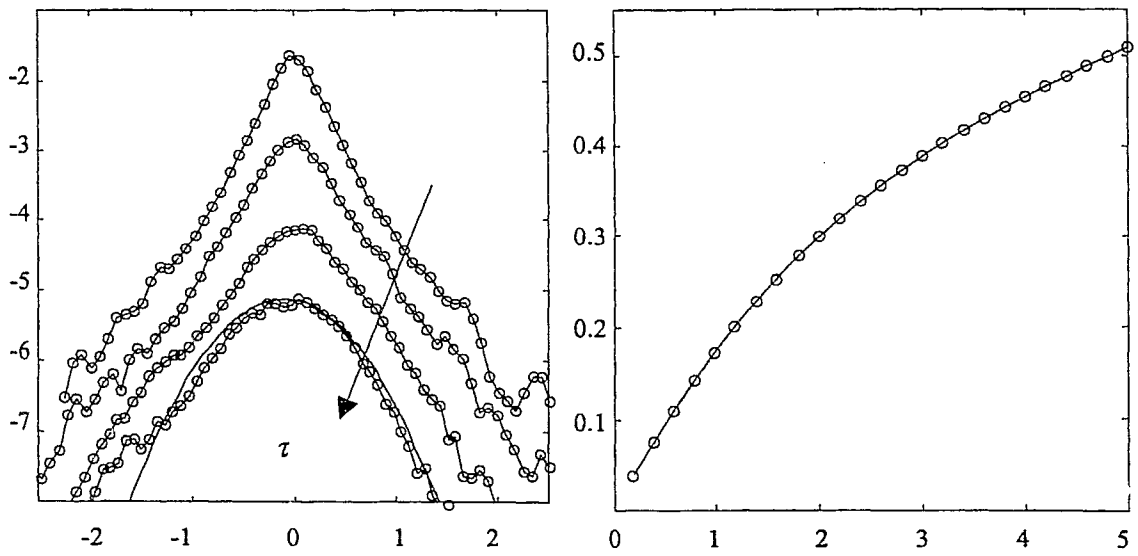

Figure 9. Simulated HRV phenomenology. (a) Simulated increment PDF $\log_2(f_\tau(\Delta r_J))$ versus Δr_J at $\tau = 2^2, 2^6, 2^{10}, 2^{14}$ (increasing in the arrow direction) and (b) $\zeta(p)$ for p = 0.2, 0.4... 5. Note that the shown increment PDF's were rescaled as in Figure 4 to give a clearer illustration. A Gaussian profile (solid line) was added to show the SEG transition at $\tau = 2^{14}$.

1.5 Overview of Thesis

This thesis contains five Chapters and two Appendices. Chapter 2 describes the application of fluid turbulence hierarchy in HRV. First the hierarchy in the context of turbulence is reviewed. Then the idea is applied in HRV. Finally, the empirical evidence of the hierarchy in HRV is presented. Chapter 3 describes the detail of the new HRV

model motivated by the existence of the hierarchy. First feedback is introduced into the HRV modeling. Then how such additive mechanisms may be integrated into the cascade structure is introduced. Finally, the numerical experiments to be carried out by the new HRV model are formulated. Numerical results are presented in Chapter 4 where the known HRV phenomenology from the model simulation data is examined and that the existence of the hierarchy in the model is verified. Conclusion and future works are given in Chapter 5.

Chapter 2

The Hierarchical Structure in HRV

In this Chapter, the turbulence analogy of HRV is further exploited and the evidence of a hierarchical structure in the ambulatory daytime RRi taken from healthy subjects is presented. The hierarchy, first proposed by She and Leveque (SL) to understand the statistical properties of turbulent flows [18], provides a successful framework to characterize the deficiency of the Kolmogorov's fluid turbulence theory. In section 2.1, the hierarchy in its fluid turbulence context is reviewed. In section 2.2, the idea of turbulence hierarchy is applied to HRV and the evidence of a HRV hierarchy in the RRi from healthy subjects is showed. In section 2.3, the only known cascade solution that solves the SL hierarchy exactly is introduced. The HRV model proposed in this research is motivated by this solution.

2.1 Introduction to Moment Hierarchy in Turbulence

The SL hierarchy in turbulence implies, over the length scale l,

$$\left(\frac{S_{p+2}(l)}{S_{p+1}(l)}\right) = A_{p+1}\left(\frac{S_{p+1}(l)}{S_p(l)}\right)^{\beta} S^{\infty}(l)^{1-\beta} \tag{9}$$

where $0 \le \beta \le 1$ is a parameter of the hierarchy, A_p, a function of p, $S_p(l) = \left\langle |\Delta v(l)|^p \right\rangle$, the pth order moment of the velocity increment $\Delta v(l) = v(l_0 + l) - (l_0)$, $S^\infty(l) \equiv \lim_{p\to\infty} S_{p+1}(l)/S_p(l)$ and $\langle \bullet \rangle$ denotes statistical average. Physically, the hierarchy captures the law of energy cascade from the large scale to the small scale. Since $S^\infty(l)$ is dominated by the statistics of large $\Delta v(l)$, it characterizes the most intense fluctuation in the turbulence field. Given the scaling law $S_p(l) \sim l^{\zeta(p)}$, the hierarchy implies the scaling model [18]:

$$\zeta(p) = h_0 p + C(1 - \beta^p) \tag{10}$$

where h_0, C are two other parameters of the hierarchy.

Substituting (10) in to (9) and using $S_p(l) \sim l^{\zeta(p)}$ can verify the scaling model and bring further interpretations of the other parameters. Specifically, the ratios of the structure functions can now be given by:

$$\frac{S_{p+1}}{S_P} = \frac{l^{\zeta(p+1)}}{l^{\zeta(p)}} = \frac{l^{h_0(p+1)+C\left(1-\beta^{p+1}\right)}}{l^{h_0 p + C\left(1-\beta^p\right)}} = l^{h_0 + C\beta^p(1-\beta)} \tag{11}$$

$$\frac{S_p}{S_{P-1}} = \frac{l^{\zeta(p)}}{l^{\zeta(p-1)}} = \frac{l^{h_0 P + C\left(1-\beta^p\right)}}{l^{h_0(P-1)+C\left(1-\beta^{p-1}\right)}} = l^{h_0 + C\beta^{p-1}(1-\beta)} \tag{12}$$

Substituting (11) and (12) into (9) shows that the hierarchy can be established if and only if $S^\infty(l) = l^{h_0}$. Hence, h_0 is the scaling exponent for the most intense fluctuation in the turbulence field. In fluid turbulence, the parameter C measures the *codimension* of the physical space which is occupied by the flow showing the most intense fluctuation [18].

It thus quantifies the size of the neighboring space surrounding the most intense structure in the turbulence flow. In isotropic turbulence, a one-dimensional vortex has been suggested to represent such a violent structure. Hence, the corresponding C parameter equals $3 - 1 = 2$. Since the equation of motion of cardiovascular dynamical system has not yet been written down, it is not possible to give a geometrical meaning to the C parameter in HRV. In this thesis, it will only be considered as a *codimension parameter*.

2.2 Experimental Evidence of She-Leveque Hierarchy in Healthy HRV

Based on the turbulence analogy (section 1.3) and the empirically observed $S_p(\tau) \sim \tau^{\varsigma(p)}$ in HRV, it is reasonable to assume that the hierarchy exists. The purpose of this section is to first formulate the hierarchy analysis in HRV and then to present evidence of the hierarchy in RRi from healthy subjects.

To apply the turbulence hierarchy to HRV, the following comparison is made: RRi versus velocity and the temporal scale (τ) versus the spatial scale (l). Hence, by hierarchy, it means that the same moment relationship (9) applied to the RRi structure function, namely, using $S_p(\tau) = \left\langle |\Delta r(\tau)|^p \right\rangle$ and substituting τ for l in (9).

To check the hierarchy, consider for a pair of fixed τ_1 and τ_2:

$$\left[\frac{S_{p+2}(\tau_1)}{S_{p+1}(\tau_1)}\right] = A_p \left[\frac{S_{p+1}(\tau_1)}{S_p(\tau_1)}\right]^{\beta} S^{\infty}(\tau_1)^{1-\beta} \qquad (13)$$

$$\left[\frac{S_{p+2}(\tau_2)}{S_{p+1}(\tau_2)}\right] = A_p\left[\frac{S_{p+1}(\tau_2)}{S_p(\tau_2)}\right]^{\beta} S^{\infty}(\tau_2)^{1-\beta} \tag{14}$$

Dividing (14) by (13) yields

$$\left[\frac{S_{p+2}(\tau_2)/S_{p+1}(\tau_2)}{S_{p+2}(\tau_1)/S_{p+1}(\tau_1)}\right] = \left[\frac{S_{p+1}(\tau_2)/S_p(\tau_2)}{S_p(\tau_1)/S_p(\tau_1)}\right]^{\beta}\left[\frac{S_{\infty}(\tau_2)}{S_{\infty}(\tau_1)}\right]^{1-\beta} \tag{15}$$

If (9) holds, then (15), considered as a function of p, describes a power law with the scaling exponent given by β.

To apply this result, 9 sets of ambulatory RRi recording taken from healthy subjects conducting normal daily activities were used. The actual recording was carried out in 24 hours in The Cardiovascular and Respiratory Dynamics Laboratory at the Kinesiology Department of the University of Waterloo. The participating subjects are volunteers that do not have any record of heart problems (mean age: 25, mean height: 174 cm, mean weight: 74 kg). A standard 2-lead electrocardiogram (ECG) recording was applied with a sampling rate of 1000 Hz. The demonstrations given in Chapter 1 are taken from this database.

Define

$$V_{\tau_1\tau_2}(p) = \left(S_{p+1}(\tau_2)/S_{p+1}(\tau_2)\right)/\left(S_p(\tau_1)/S_p(\tau_1)\right)$$

and the power law relationship in (15) is written as

$$V_{\tau_1,\tau_2}(p+1) \sim V_{\tau_1,\tau_2}(p)^{\beta} \tag{16}$$

Equation (16) was used to check the hierarchy as well as to estimate the β. The numerical results are summarized in Table 1. It is seen a wide range of β values (0.6~0.9) is covered. The exact implication of the large β variation in physiology terms is not clear at this time. Using the typical RRi data in Chapter 1, Figure 10 and Figure 11 further show consistent β estimates over different sets of τ_1 and τ_2 (Table 2 and Table 3), indicating a genuine hierarchical structure in healthy HRV.

Table 1. Numerical Results for Hierarchy

No. of Subjects	1	2	3
β Value	0.7480	0.8522	0.7555
No. of Subjects	4	5	6
β Value	0.8016	0.8748	0.6543
No. of Subjects	7	8	9
β Value	0.7724	0.8418	0.7305

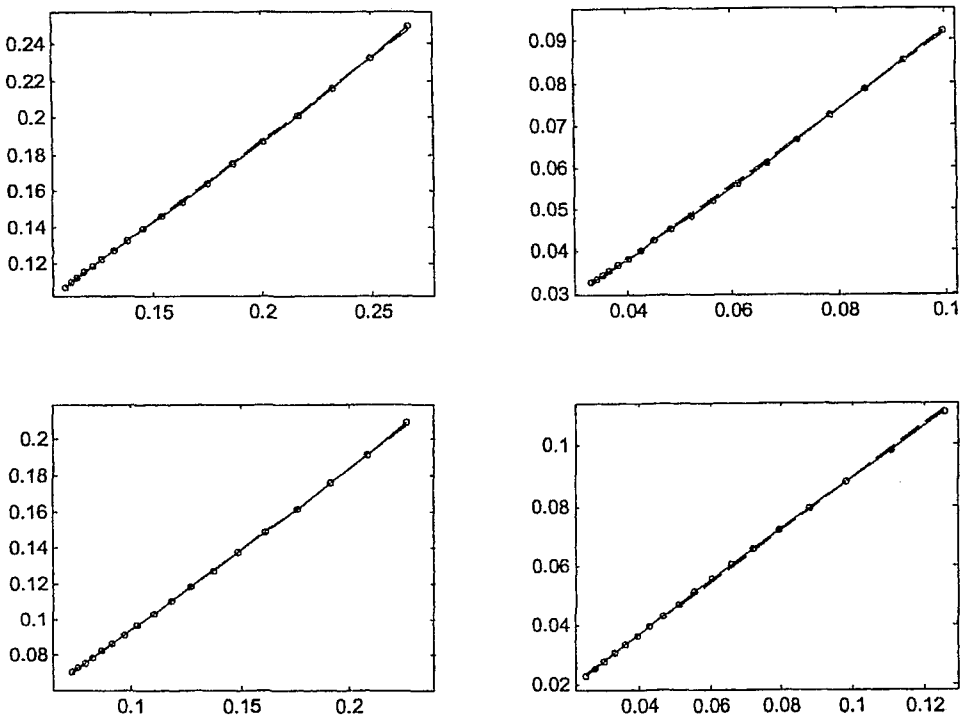

Figure 10. The plot of $V_{\tau_1,\tau_2}(p+1)$ versus $V_{\tau_1,\tau_2}(p)$ on base 2 log-log scales from a typical RRi data set for p = 0.25, 0.5, ..., 5. The solid line is the connecting line between data points and the dash line is the fitting line. See Table 2 for other parameters.

Table 2. β values for different τ_1 and τ_2

$\tau_1=2^5,\tau_2=2^{12},\beta=0.64066$	$\tau_1=2^7,\tau_2=2^{10},\beta=0.64082$
$\tau_1=2^4,\tau_2=2^{10},\beta=0.63824$	$\tau_1=2^5,\tau_2=2^8,\beta=0.60207$

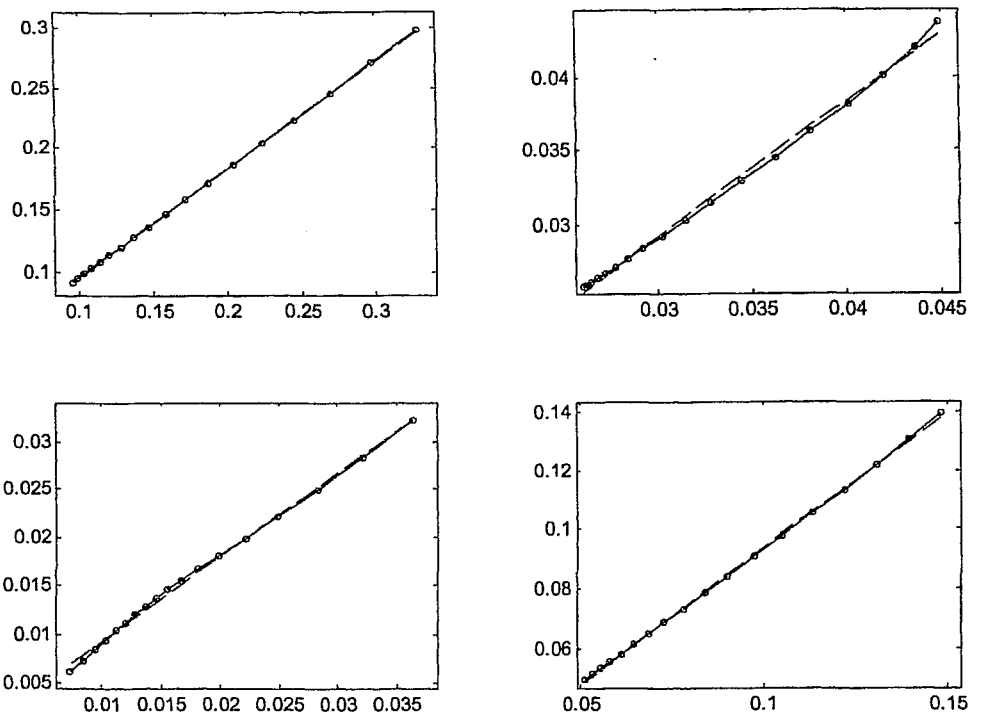

Figure 11. The plot of $V_{\tau_1,\tau_2}(p+1)$ versus $V_{\tau_1,\tau_2}(p)$ on base 2 log-log scales from a typical RRi data set for p = 0.25, 0.5, ..., 5. The solid line is the connecting line between data points and the dash line is the fitting line. See Table 3 for other parameters.

Table 3. β values for different τ_1 and τ_2

$\tau_1=2^3,\tau_2=2^{11},\beta=0.59887$	$\tau_1=2^6,\tau_2=2^7,\beta=0.69664$
$\tau_1=2^5,\tau_2=2^6,\beta=0.58007$	$\tau_1=2^8,\tau_2=2^{12},\beta=0.71191$

2.3 The She-Waymire Cascade

The She-Waymire (SW) cascade is an exact solution to the SL hierarchy [17]. The philosophy of the SW cascade forms the basis of the HRV model proposed in this thesis. In this section, the main ingredients of the SW cascade and its relationship with the SL hierarchy will be briefly covered. These ideas in Chapter 3 will be applied to develop the HRV model.

SW cascade is similar to the regular cascade but has a different construction of its cascade components. Since it has its origin in fluid turbulence, spatial scale l will be used again in this section.

The SW cascade assumes, for arbitrary scales l, l_n, that the cascade is given by

$$W_{ll_n} = \left(\prod_{m=l}^{l_n} \omega_m \right) \beta^Y \tag{17}$$

where $\beta \leq 1$ is the same parameter used in the SL hierarchy Equation (9) and Y is a Poisson random variable. Since $0 < \beta \leq 1$, the multiplicative of β^Y can be considered as a modulating event. She and Waymire described this term as "defect dynamics," since it creates the effect of dampening the fluctuation.

The pth order moment of W_{ll_n} can be written as,

$$\log \left\langle \left| W_{l l_n} \right|^p \right\rangle = \log \left\langle \left| \prod_{m=l_n}^{l_n} \omega_m \right|^p \right\rangle + \log \left\langle \left| \beta^{Yp} \right| \right\rangle \tag{18}$$

Using the PDF of the Poisson variable with a density λ,

$$f_Y(y) = \exp(-\lambda)\frac{\lambda^y}{y!}, \tag{19}$$

the moment of $\log\left\langle \left| \beta^{Yp} \right| \right\rangle$ can be found to be

$$\lambda(\beta^p - 1) \tag{20}$$

based on the following transformation rule between the PDF's of Y and β^Y. Let $X = \beta^Y$. Then, $\log(X)/\log(\beta) = Y$ and there is the relationship between the PDF's $f_X(x)$ and $f_Y(y)$:

$$f_X(x) = f_Y(\log(x)/\log(\beta))\left(\frac{1}{x}\right)\left(\frac{1}{\log(\beta)}\right). \tag{21}$$

Equation (20) can be obtained by substituting (19), (21) into the definition of a moment. For SW cascade, the corresponding $\{\omega_m\}$ are assumed independent ,and $\left\langle W_{l l_n} \right\rangle = 1$. From these two assumptions, the moment of $\left\langle \left| \omega_l ... \omega_{l_n} \right|^p \right\rangle$ has a scale-dependent power law relationship:

$$\left\langle \left| \omega_l ... \omega_{l_n} \right|^p \right\rangle \sim (l/l_n)^{\gamma p} \tag{22}$$

where γ is a constant (Appendix A). Substituting the above and (20) into (18) yields

$$\log\left(\left\langle \left|W_{ll_n}\right|^p \right\rangle\right) = \gamma p \log\left(\frac{l}{l_n}\right) + \lambda(\beta^p - 1) \tag{23}$$

The assumption $\left\langle W_{ll_n} \right\rangle = 1$ dictates the value of λ to be

$$\lambda = -\frac{\gamma \log(l/l_n)}{\beta - 1}. \tag{24}$$

Letting $(l/l_n)^\gamma = \chi$ and using (24), (23) can now be written as

$$\log \left\langle \left|W_{ll_n}\right|^p \right\rangle \sim \left(p - \frac{\beta^p - 1}{\beta - 1}\right) \log \chi \tag{25}$$

It is now straightforward algebra to show

$$< W_{l l_n}^{p+1} > / < W_{l l_n}^{p} > = \chi^{1-\beta^p}. \tag{26}$$

Similarly,

$$< W_{l l_n}^{p} > / < W_{l l_n}^{p-1} > = \chi^{1-\beta^{p-1}}. \tag{27}$$

Equations (26) and (27) imply the exact form of SL hierarchy (9)

$$< W_{l l_n}^{p+1} > / < W_{l l_n}^{p} > = [< W_{l l_n}^{p} > / < W_{l l_n}^{p-1} >]^{\beta} \chi^{1-\beta}. \tag{28}$$

Note that $\chi = (l/l_n)^\gamma$ characterizes the $S^\infty(l)$ in the hierarchy of SW cascade.

The significance of the SW cascade is that it is the first time SL hierarchy was exactly solved. The importance of including the modulating component is evident as it contributes to the extra term in (20), which in turn leads to the exact SL hierarchy form in (28).

The Poisson assumption may be generalized so long as

$$\log\left(\left\langle \left|W_{ll_n}\right|^p \right\rangle\right) = g(p;\beta) + \log(\chi) \tag{29}$$

where $g(p; \beta)$ satisfies the following condition:

$$g(p;\beta) - g(p+1;\beta) \sim \beta^p. \tag{30}$$

Chapter 3

The Local-Feedback-Global-Cascade Model

3.1 Motivation

Biological systems normally rely on feedback mechanisms to achieve local regulations that can sometimes create system-wide effects. For example, regional increase of the mean arterial pressure will be sensed and regulated by the vascular system. When the effect of blood pressure increase reaches major barorecepter sites, the effect of feedback regulation may be sent to the cardiovascular centers in the brain stem to bring about a slower heart rate.

The feedback action is in principle governed by additive laws. Although cascade is able to capture HRV phenomenology very well (section 1.3.2), the additive mechanism is completely missing in its construction. The main objective of the model introduced in this Chapter is to integrate an additive law as local feedback into the cascade. Such a model is called a local-feedback-global-cascade (LFGC) model.

The way the feedback is introduced into the cascade is largely motivated by the empirical observation of SL hierarchy (section 2.2) and the philosophy of the SW cascade. In particular, the modulating effect in the SW cascade is simulated by using feedback. First, the feedback mechanism will be introduced in section 3.2. In Section 3.3, its integration

with the cascade structure will be described. Finally, the numerical experiments to be executed by the LFGC will be given in section 3.4.

3.2 The Local Feedback Law in LFGC

As motivated by the SW cascade, the objective of the feedback in LFGC model is to reduce the fluctuation of the cascade component. The novelty of the model is the introduction of a scheduling law, which determines the timing of the feedback activation for the cascade components. Specifically, the following four assumptions form the basis of the feedback control in LFGC model:

A. There exist control set points $V_j, j = 1,2, \ldots, J$, for the feedback on the cascade component.

B. The control is "one way" based on the a scheduling law: namely, the control applied to the cascade component of the jth generation is *scheduled* by the cascade component of the $(j-1)$th generation. Hence, it can be said the control is "directed" from the large to the small time scale components.

C. The scheduling law is defined by the branching rule of the cascade: namely, the control from the $(j-1)$th generation to the jth generation will take effect *only* at the instants when ω_{j-1} changes its value.

D. The feedback control is a "mean-field" type position feedback. The objective is to bring the cascade component ω_j closer to the mean value μ_j according to

$$\omega_j(t) = \mu_j + \mathbf{w}\sigma_j(V_j - B_{j-1}) \tag{31}$$

where w is a the same Gaussian variable defined in the bounded cascade model (Section 1.3.2) and, for $t_n = n\delta_{j-1}$, $n = 1, 2, \ldots$,

$$B_{j-1} = \left\langle \left| \omega_j(t) - V_j \right| \right\rangle = \left(\sum_{t=t_n}^{t_n+\delta_{j-1}} \left| \omega_j(t) - V_j \right| \right) \Big/ \delta_{j-1} \tag{32}$$

It is seen that the feedback quantity, as determined by the B_{j-1} parameter, is the average of the absolute difference between $\omega_j(t)$ and the control set point V_j. In this work, V_j will be set to be close to μ_j and $V_j \gg \sigma_j$. Hence, when there is a large deviation of $\omega_j(t)$ from V_j, B_{j-1} will be large. As a result, $\omega_j(t)$ after control will tend to its mean value μ_j as the factor $(V_j - B_{j-1})$ in (31) tends to be smaller.

3.3 Integrating feedback to cascade

The integration of the local feedback into the cascade can be best described by the simulation algorithm of the LFGC time series provided in Figure 12. The actual implementation is carried out by the numerical package MATLAB [19].

The simulation starts by initializing the parameters J, $\sigma_j, \mu_j, V_j, j = 1, \ldots, J$. The calculation starts at $t = 1$ and ends some pre-set terminal time t = N. The cascade component

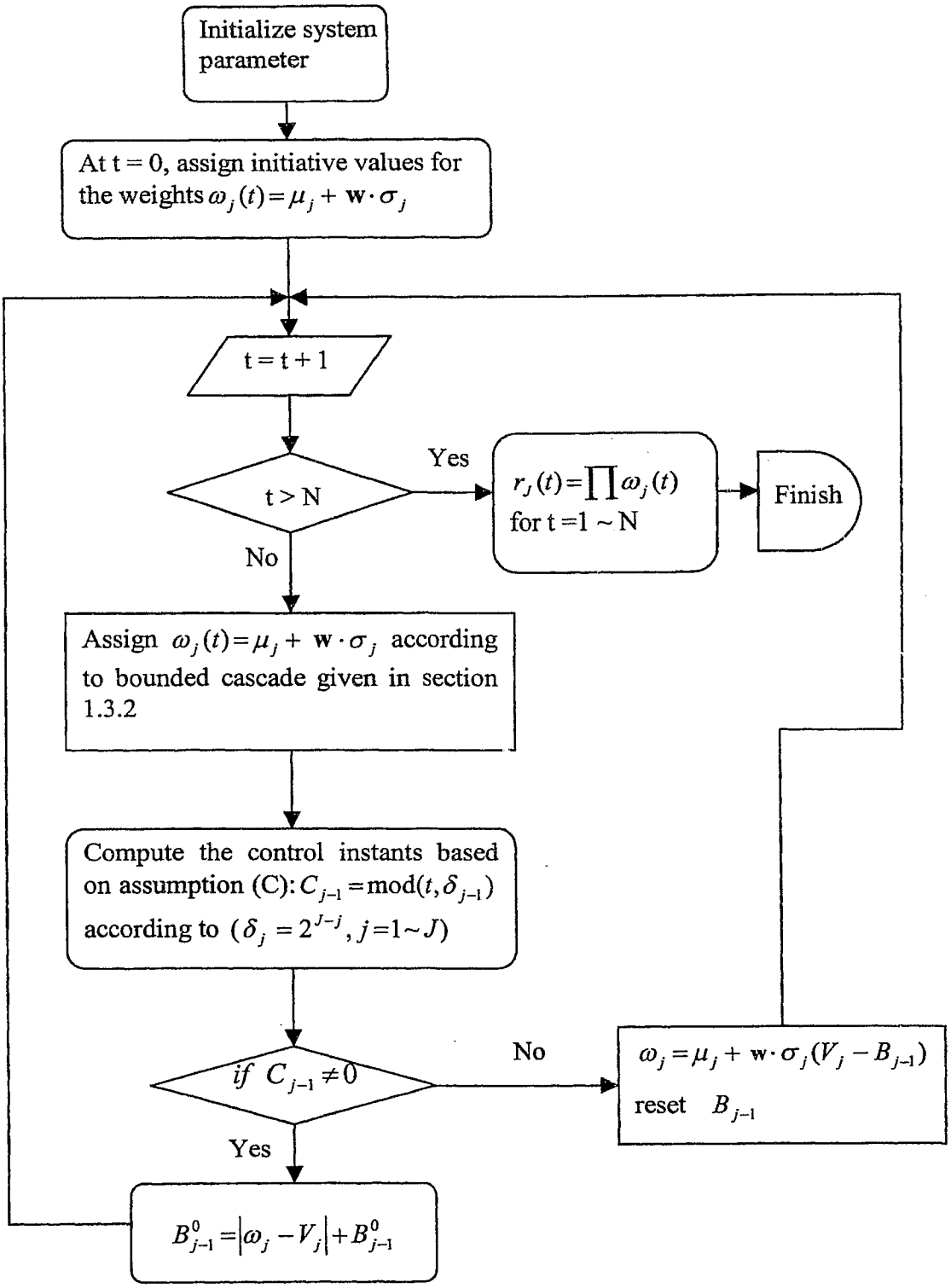

Figure 12. Program Flowchart for LFGC model

ω_j is updated randomly according to the branching rule introduced in Section 1.3.2. The feedback control is applied at the instant determined by the scheduling law according to (29). The time for control application is determined based on the assumption C in the previous Section. In numerical simulation, it can be easily found by using the mod-function in MATLAB, i.e. the control is applied whenever mod $(t, \delta_{j-1}) = 0$ (recall $\delta_j = 2^{(J-j)}, j = 1, \ldots, J$). Figure 13 shows the schematics of the scheduling law. This process will repeat until the terminal time $t = N$ is reached. Then, the simulated LFGC time series $r_J(t)$ is obtained by the product $\prod_{j=1}^{J} \omega_j$.

3.4 Numerical Experiments

To study the LFGC model, it was considered as being parameterized by four sets of parameters: $\{V_j,\ j = 1 \sim J\}$, $\{\mu_j, j = 1 \sim J\}$, α and σ_0.

These parameters are varied in the numerical experiment described in this section. For each selected set of parameters, 100 LFGC time series were generated and used to form the ensemble for studying increment PDF, structure function and hierarchy.

In order to make systematic comparisons, the reference using $V_j = 1$, $\mu_j = 1$, $\alpha = 0.2$ and $\sigma_0 = 2^{-1.5}$ is defined and is called *control case*. This set of parameters was found to capture HRV phenomenology in healthy state very well; see Section 1.3.2.

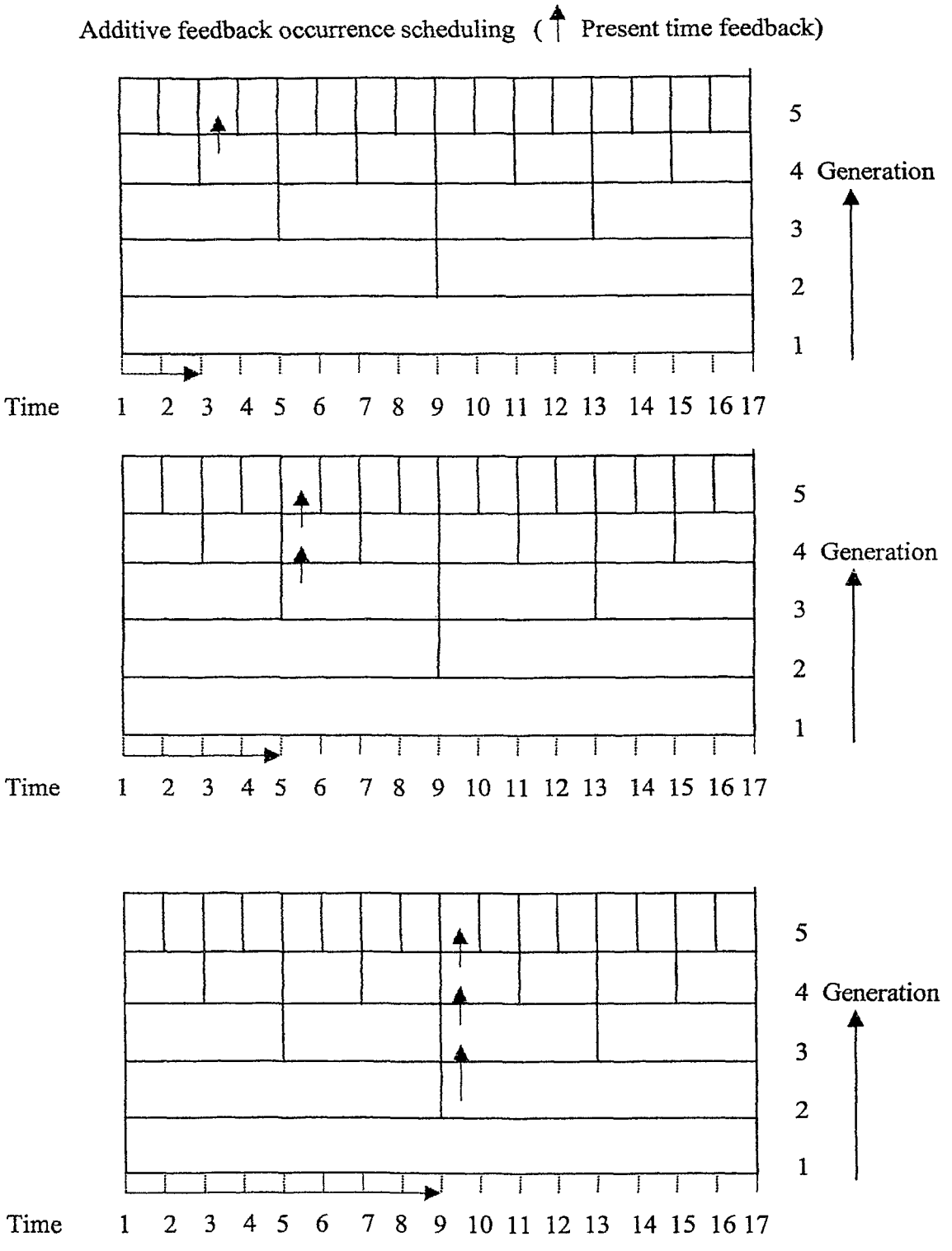

Figure 13. Schematic diagram of Additive feedback in cascade model

The numerical experiments conducted in this thesis consist in varying the α and μ parameters of the model. For the α parameter, it is varied in the range of 0.1 to 0.3 with increment $\Delta\alpha = 0.025$ (a total of 9 cases). The corresponding model set is referred to as the α-group. For the μ parameter, it is varied from 0.4 to 1.6 with increment $\Delta\mu = 0.2$ (a total of 7 cases) and the corresponding model set is referred to as the μ-group.

The α-group is designed to study the qualitative change of the scaling property under the influence of the feedback. It can be shown that the multiplicative mechanism turns into an additive one as α increases [5]. This is due to the fact $\sigma_j = \sigma_0 2^{-\alpha(j-1)}$ and $\sigma_j \ll 1$ for large α, in which case,

$$r_J(t) = \prod_{j=1}^{J} \omega_j \sim 1 + \sigma_1 \mathbf{w} + \sigma_2 \mathbf{w} + \ldots + \sigma_J \mathbf{w}$$

by dropping the higher order terms. It is thus clear $r_J(t)$ is formed by adding random variables on the dyadic tree. For small p, it has been found that the structure function is scaled by a linear $\zeta(p)$ [4, 5]:

$$S_p(\tau) \sim \tau^{\alpha p}.$$

This means the α parameter can induce a qualitative change on the scaling property of $r_J(t)$. The purpose of studying the $\alpha-$group is to document the change in scaling property under the influence of feedback in LFGC.

The study of the μ-group allows us to examine the effect of mismatch between the μ_j's, the controlled value for the cascade component, and the V_j's, the control set points by which the control quantity is determined. The simulation results of these experiments will be given in the next Chapter.

Chapter 4

Simulation Results

In this chapter, the simulation results of the LFGC model described in Chapter 3 will be reported. First, the simulation of HRV phenomenology summarized in section 1.2 will be shown. Then, evidence of hierarchy of the SL type will be presented. All computed quantities in the α - and μ -groups were averaged from the ensemble of 100 sets of LFGC generated time series $r_j(t)$ of the corresponding parameter setting.

4.1 LFGC phenomenology

In this section, the phenomenology exhibited by the LFGC generated will be presented. As shown below, the LFGC phenomenology given in this section is consistent with those observed in the real data summarized in section 1.2.

A. 1/f power law

It may be expected that the 1/f-like power spectrum continues to hold in the LFGC generated data since self-similarity was built-in by the branching rule of the cascade. Indeed, Figures 14 and 15 show such a 1/f law in the simulated data taken from the α – and μ –groups respectively. It is seen that a larger α leads to a larger 1/f spectral exponent.

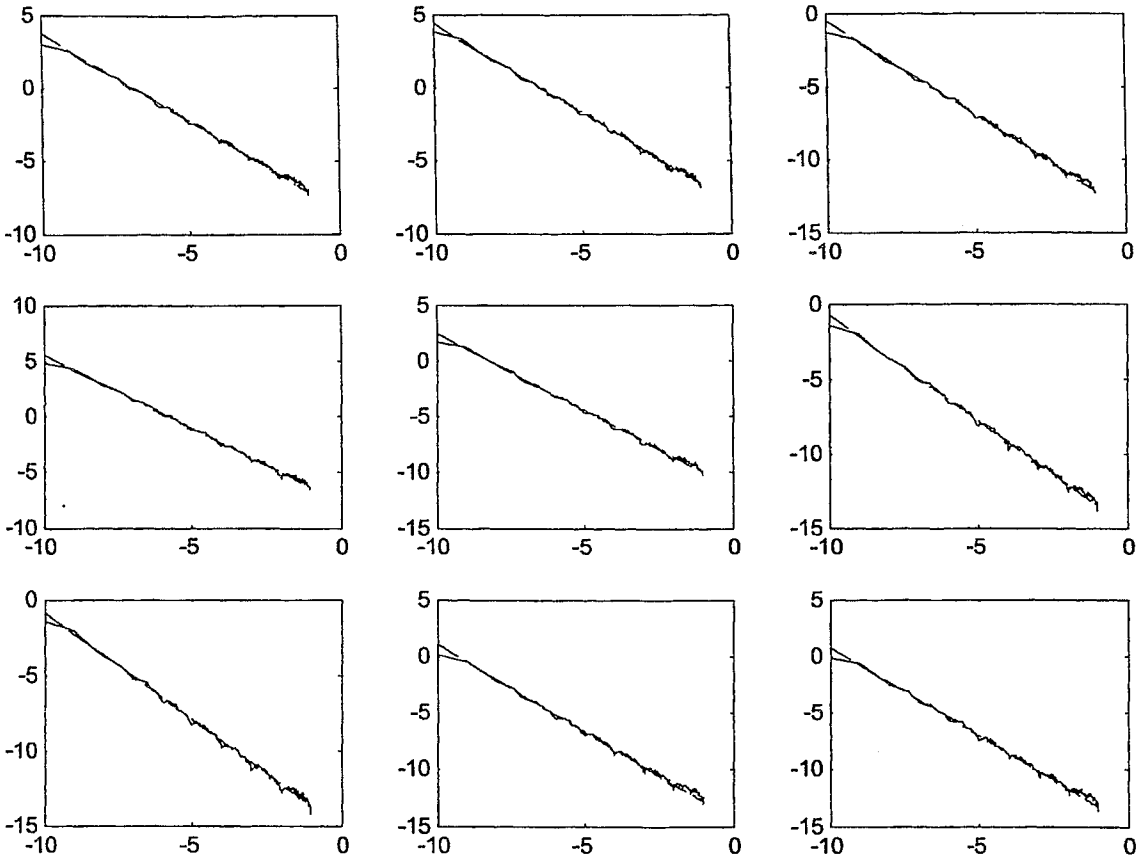

Figure 14. Power spectrum in the α group of LFGC model. From left to right in the first row: α = 0.1, 0.125, 0.15, the second row: α = 0.175, 0.2, 0.225, the third row: α = 0.25, 0,275, 0.3. In each subfigure Abscissa: $\log_2(f)$; Ordinate: $\log_2(P)$; solid line: power spectrum, dash line: fitting line.

A proportional relationship between the α value and the 1/f spectral exponent is found; see Figure 16. But, for the μ - group, no identifiable relationship between ρ and μ is indicated (Figure 17).

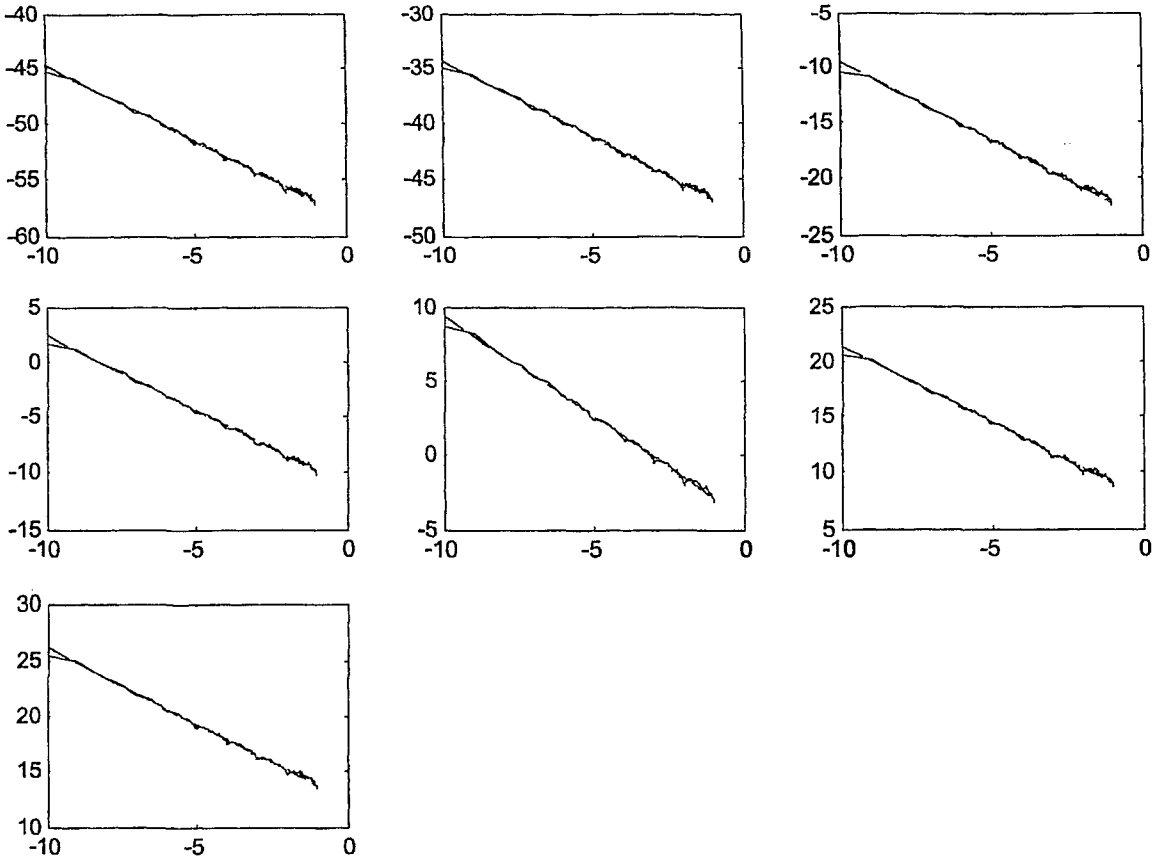

Figure 15. Power spectrum in the μ group of LFGC model. From left to right in the first row: μ = 0.4, 0.6, 0.8, the second row μ = 1, 1.2, 1.4, the third row: μ = 1.6. In each subfigure Abscissa: $\log_2(f)$; Ordinate: $\log_2(P)$; solid line: power spectrum, dash line: fitting line.

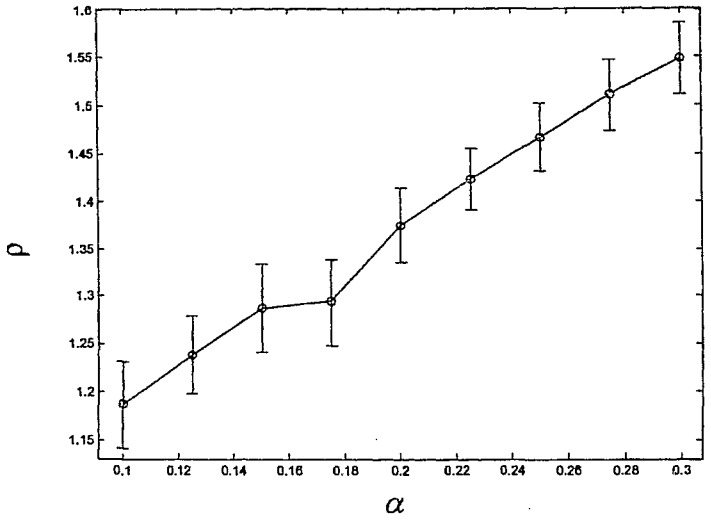

Figure 16. ρ versus α relationship. (Circle: data points, solid line: connecting line between data points, errorbar represents one standard deviation)

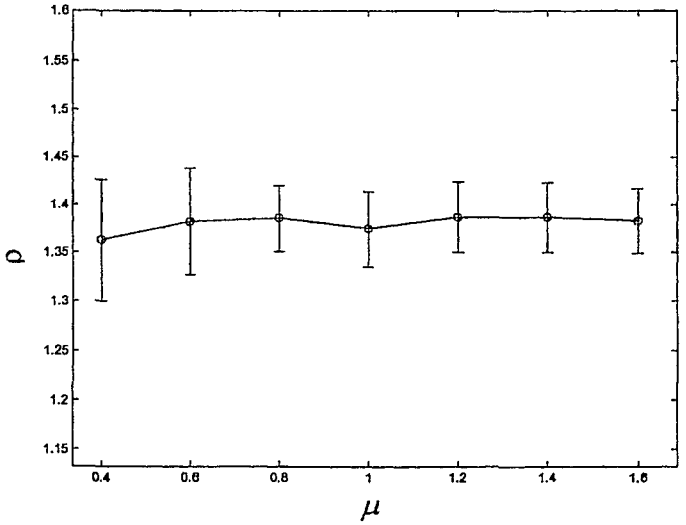

Figure 17. ρ versus μ relationship. (Circle: data points, solid line: connecting line between data points, errorbar represents one standard deviation)

B. Self-similarity

Since self-similarity is built-in from the branching rule of the cascade, the simulated LFGC time series $r_J(t)$ and the fragmented part of it should exhibit self-similarity. Figures 18 and 19 show a representative case taken from the α -group with $\{V_j = 1\}$, $\{\mu_j = 1\}, \alpha = 0.2$ and $\sigma_0 = 2^{-1.5}$. Figure 19 shows the segment in the rectangular region of Figure 18. Self-similar patterns can be seen. The 1/f-like power spectrum and the property of self-similarity imply a fractal LFGC time series $r_J(t)$. They suggest more details in the scaling of LFGC generated time series, as investigated in **C** and **D** below.

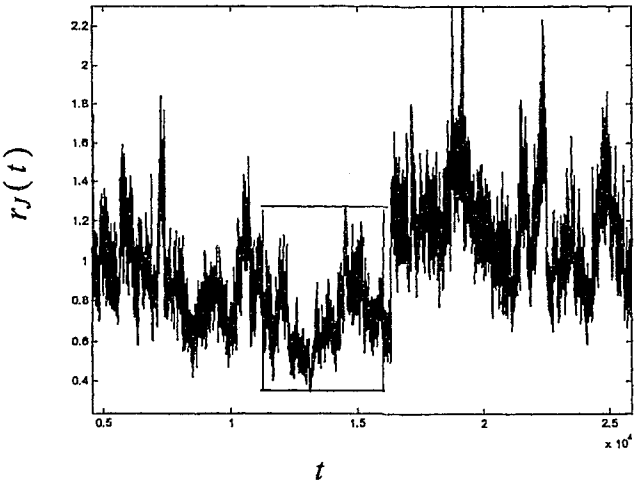

Figure 18. Representative time series $r_J(t)$. Data taken from the α group with $\{V_j = 1\}, \{\mu_j = 1\}, \alpha = 0.2$.

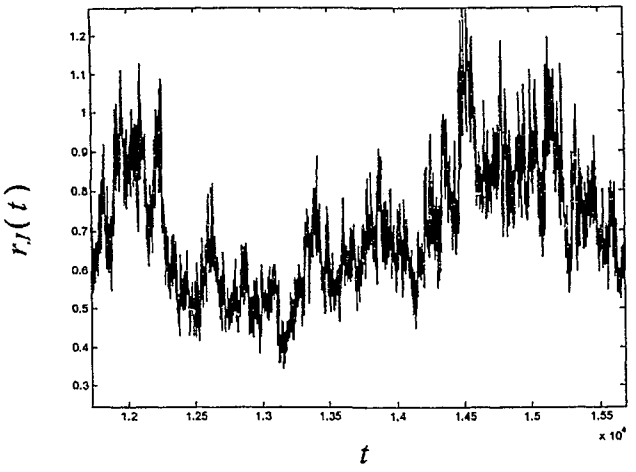

Figure 19. Rectangular region in Figure 17.

C. Increment PDF

The simulated LFGC time series $r_J(t)$ were use to calculate its increment according to (1), $\Delta r_J(\tau) = r_J(t+\tau) - r_J(t)$. The increment PDF suggests the same SEG transition as observed in Section 1.2. In what follows, the increment PDF's of the simulated time series in α - and μ -groups at different τ values are shown. Then, the kurtosis is used to compare the theoretical values of the SEG transition.

Figures 20 ~ 24 show the normalized histogram of $\Delta r(\tau)$ for $\tau = 2^0, 2^3, 2^6, 2^9, 2^{12}$ of the control case, the α -group and μ -group, respectively. In all cases, the SEG transition can be observed.

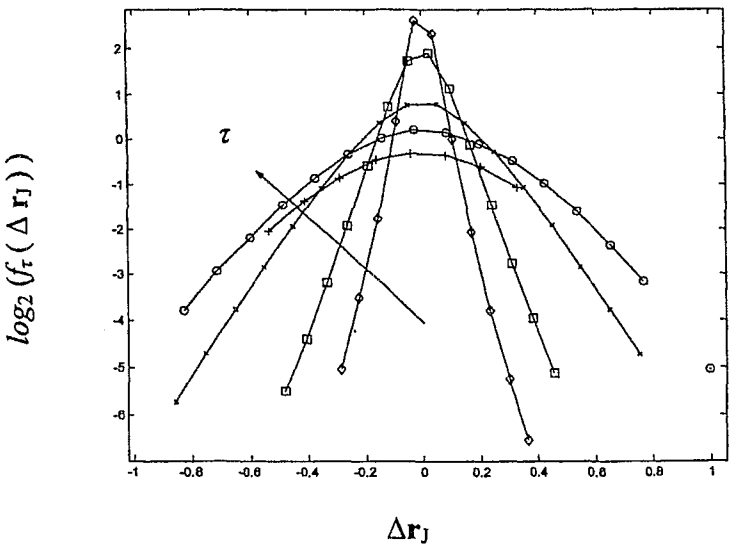

Figure 20. Increment PDF in the Control case ($V_j = 1$, $\mu_j = 1, \alpha$ = 0.2) (Solid line with diamond : $\tau = 2^0$, with square: $\tau = 2^3$, with cross: $\tau = 2^6$, with circle: $\tau = 2^9$, with plus: $\tau = 2^{12}$.).

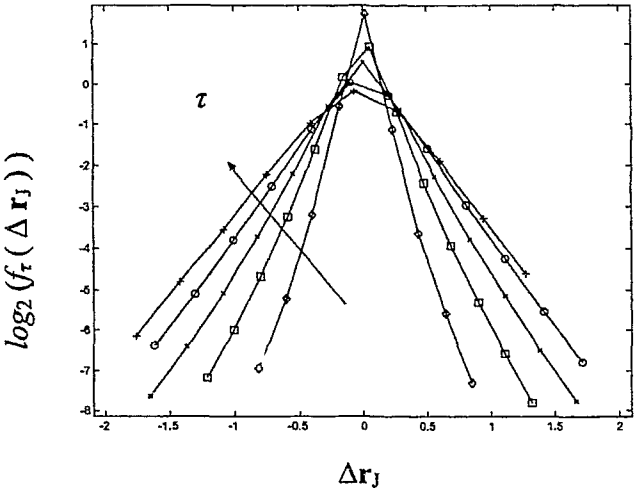

Figure 21. Increment PDF taken from the α-group with α =0.1 (Symbol designation follows the same as Figure 18.).

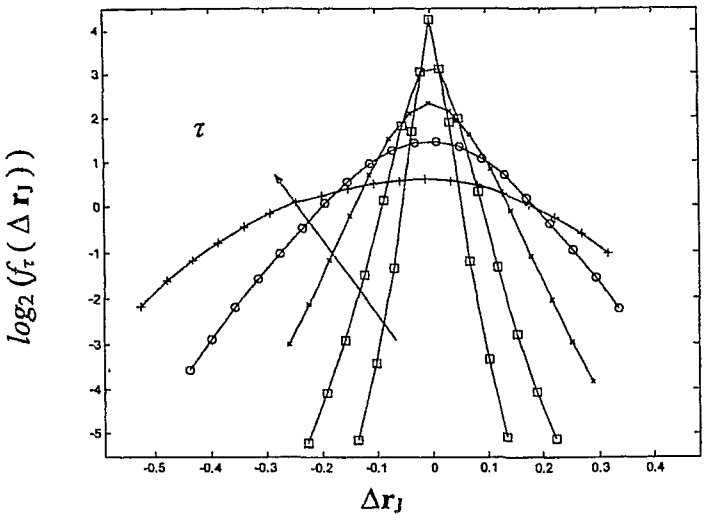

Figure 22. Increment PDF taken from the α -group with α =0.3 (Symbol designation follows the same as Figure 18.).

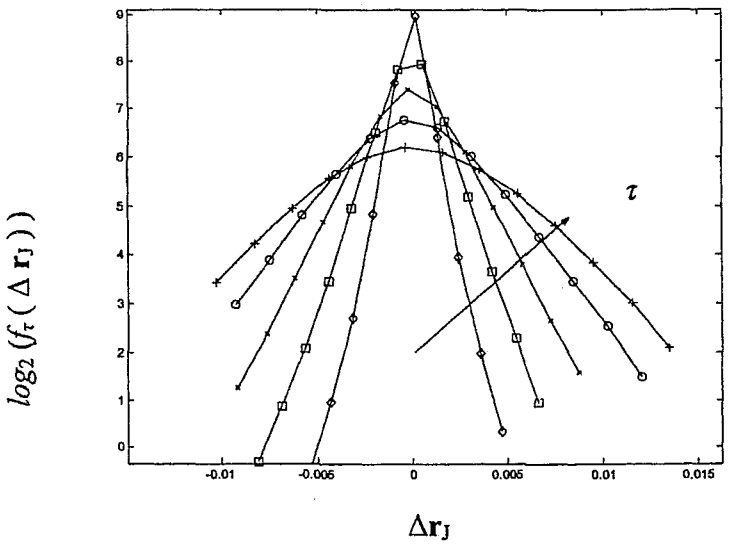

Figure 23. Increment PDF taken from the μ -group with μ =0.8 (Symbol designation follows the same as Figure 18.).

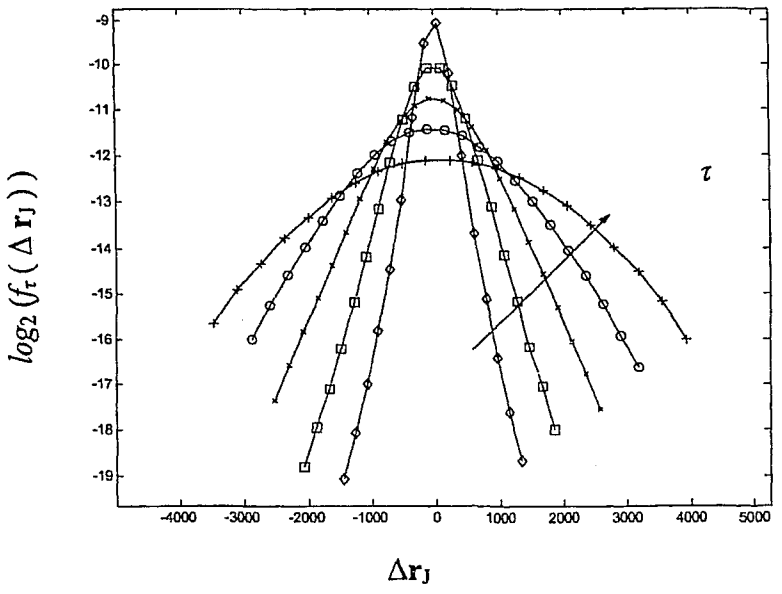

Figure 24. Increment PDF taken from the μ-group with μ=1.6 (Symbol designation follows the same as Figure 18.).

The kurtosis of the nine cases in the α-group was estimated. They are plotted on a base 2 log-log scale and superimposed in Figure 25. Similarly, the seven cases of the μ-group are shown in Figure 26. Except for $\alpha = 0.1 \sim 0.175$ and $\mu = 0.6 \sim 0.8$, all other cases exhibit the following two properties: (a) the kurtosis of the increment PDF crosses over the theoretical values from exponential to Gaussian distribution as τ increases and (b) the kurtosis exhibits a power law relationship with τ. The property (a) suggests the SEG transition and the property (b) suggests $S_p(\tau) \sim \tau^{\zeta(p)}$, following the same argument in Section 1.2.C that the structure function scaling implies $K(\tau) \sim \tau^{\gamma}$ and $\gamma = \zeta(4) - 2\zeta(2)$. As shown next, the power law structure function can indeed be found in the LFGC generated time series. For the cases which do not show these two characteristics, the kurtosis value is bigger than 3 even for the largest τ value used in the simulation.

However, the decaying kurtosis curve suggests the transition will eventually take place as the approach to the Gaussian distribution to be realized in much larger τ value. Compared with the result of the real data (Figure 5), it implies these parameter values cannot be used to simulate healthy HRV phenomenology.

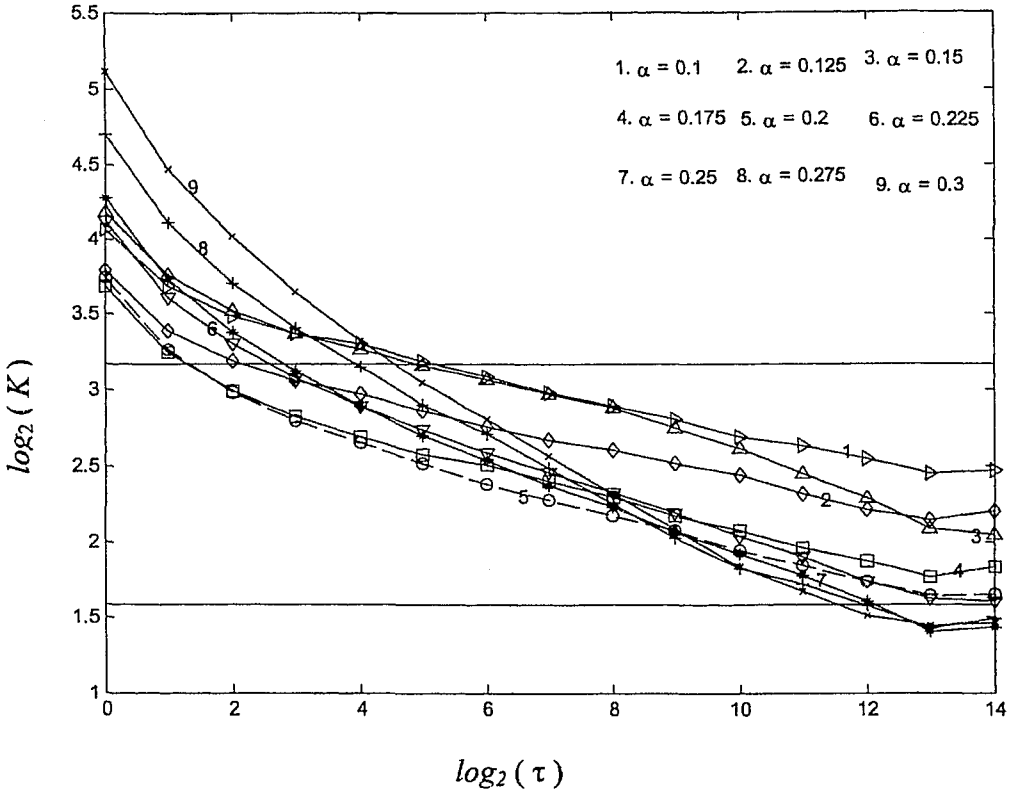

Figure 25. Kurtosis Curves of the α-group (dash line with circle: control case α = 0.2 ; solid line with triangle-right: α =0.1, with diamond: α =0.125, with triangle-upward: α =0.15, with square: α =0.175, with triangle-downward: α =0.225, with asterisk: α =0.25, with plus: α =0.275, with cross: α = 0.3.). The high horizontal line is the kurtosis value for exponential distribution and the low horizontal line for normal distribution.

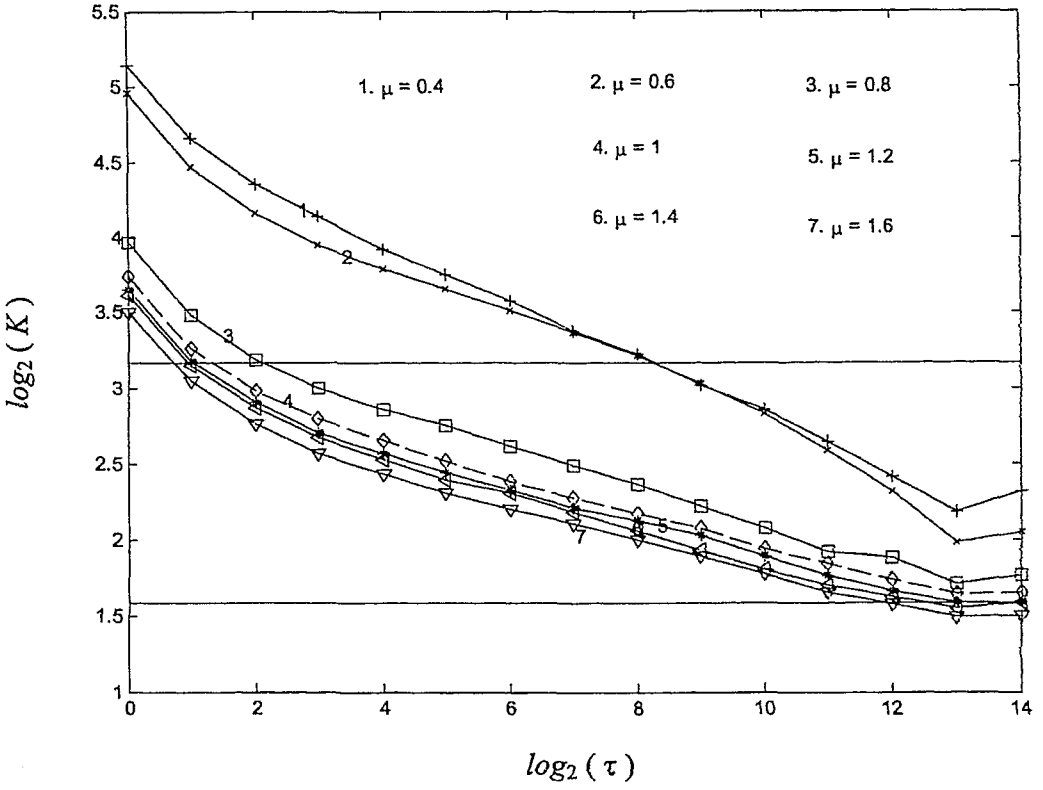

Figure 26. Kurtosis Curves of the μ-group (solid line with plus: $\mu = 0.4$, with cross: $\mu = 0.6$, with square: $\mu = 0.8$, dash line with diamond; $\mu = 1$, , solid line with asterisk: $\mu = 1.2$, with triangle-left: $\mu = 1.4$, with triangle-downward; $\mu = 1.6$.).The high horizontal line is the kurtosis value for exponential distribution and the low horizontal line for normal distribution.

D. The Scaling Exponent $\zeta(p)$ of the Structure Function

Given the kurtosis result in **C.**, now it will be confirmed that the structure function of the LFGC generated $r_j(t)$ does exhibit a power law scaling

$$S_p(\tau) \sim \tau^{\zeta(p)}$$

where $S_p(\tau) = \left\langle \left| \Delta r_j(\tau) \right|^p \right\rangle$. This is shown in Figure 27 for a typical $S_p(\tau)$ taken from the α -group.

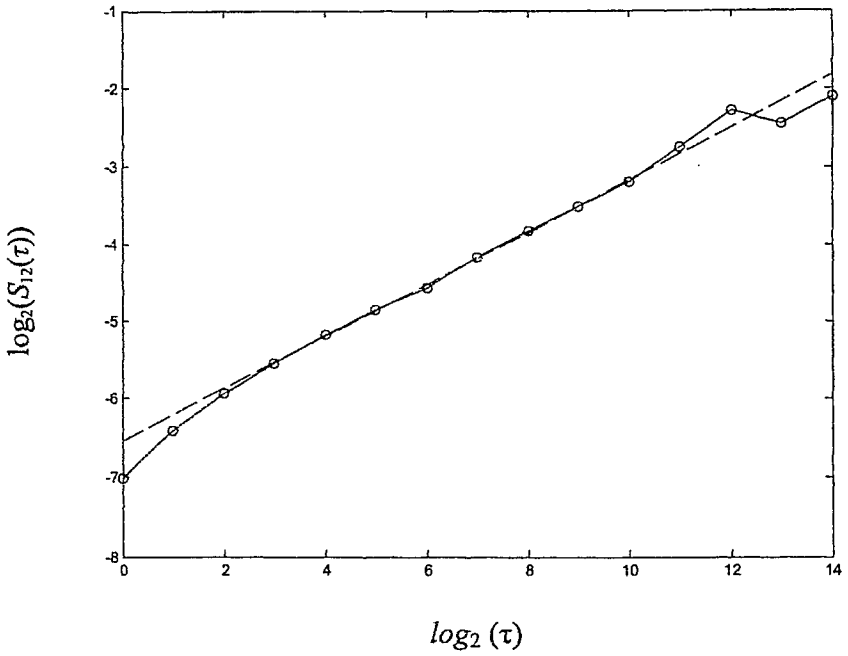

Figure 27. The power law $S_p(\tau)$ for Time series $r_j(t)$ in a simulation for $V_j = 1$, $\mu = 1, \alpha = 0.2$ .The straight line demonstrates the linear fit of the power law.

Of particular interest in the study of the power law structure function is the dependence of the scaling exponent $\zeta(p)$ on the α and μ parameters of the model. To this end, the $\zeta(p)$'s of the 100 samples in each simulation case of the α -group (9 cases) and μ -group (7 cases) were extracted. They form the ensemble to estimate the mean and standard deviation of $\zeta(p)$ for the corresponding parameter settings in these model

groups. The numerical results are summarized in Figure 28 for the α -group data and Figure 29 for the μ -group data.

Two observations can be made regarding the α -group results: (a) there is less curvature in the $\zeta(p)$ in small p as α increases and (b) there is a saturation of $\zeta(p)$ =1 in all cases and the saturation point is located at smaller p values for larger α .

The first observation (a) is consistent with the past simulation result where a larger α value results in an approximately additive model, which in turns implies a more linear $\zeta(p)$; see Section 3.3. The second observation (b) is a property of the bounded model. This is because the high order moment is dominated by large increments. Due to the boundedness of the model, there is a finite cutoff at the tails. This implies $S_{J,p}(\tau) \sim S_{p'}(\tau)$ for $p, p' \geq 1$, and thus $\zeta(p) \sim \zeta(p')$ for large p.

For the μ -group results, it is seen that the $\zeta(p)$ does not vary too much with μ . This implies the mismatch between the control set point and the mean value of ω_j is not critical for the scaling property to exist.

Figure 30 and Figure 31 show the change of the standard deviation with p in the α – and μ –group, respectively. It is seen that a larger α or μ value leads to a smaller standard deviation of $\zeta(p)$.

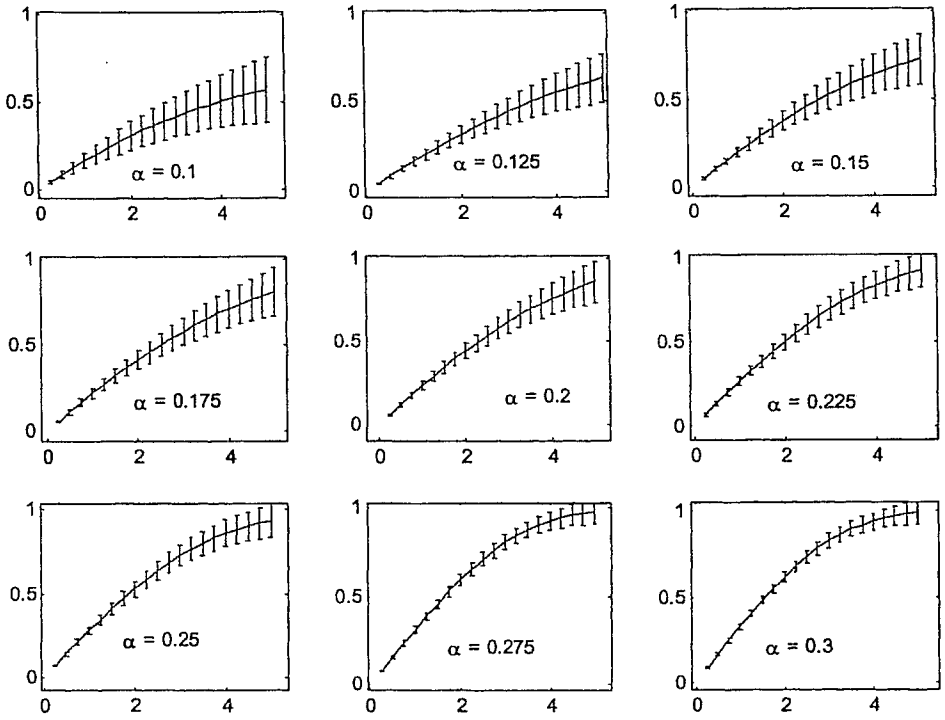

Figure 28. $\zeta(p)$ in the α group. In each subfigure, abscissa: p; ordinate: $\zeta(p)$. Confidence interval for $\zeta(p)$ is within its mean plus or minus one standard deviation.

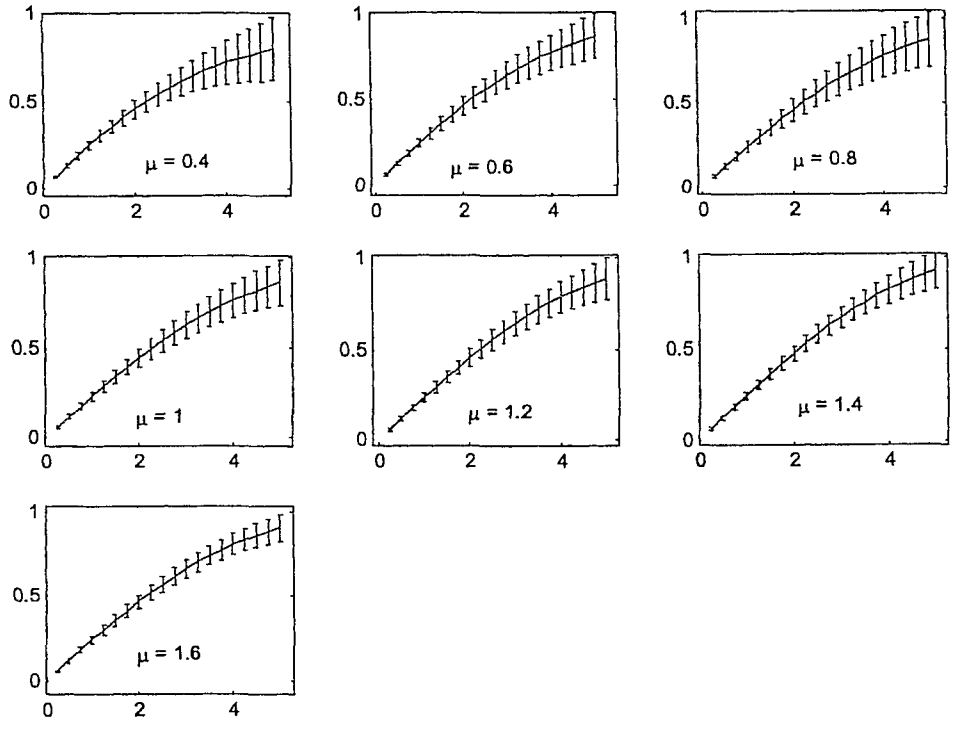

Figure 29. $\zeta(p)$ in the μ group. In each subfigure, abscissa: p; ordinate: $\zeta(p)$. Confidence interval for $\zeta(p)$ is within its mean plus or minus one standard deviation.

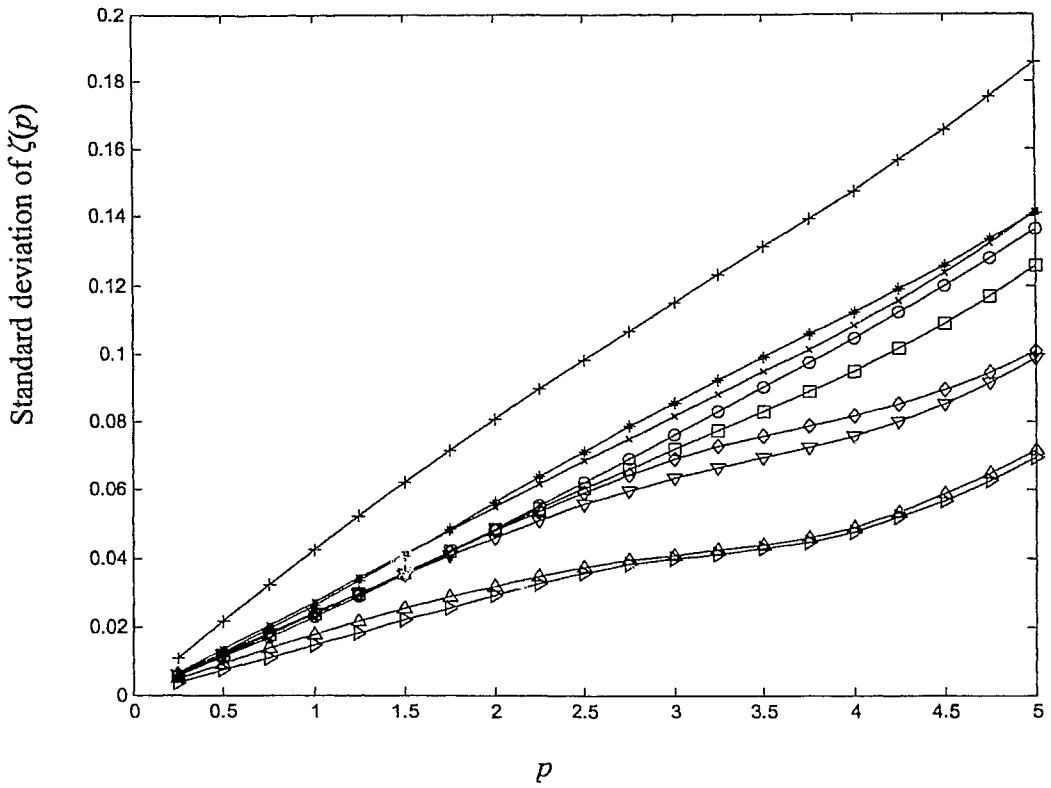

Figure 30. Standard deviation of $\zeta(p)$ versus p in α group (Solid line with plus sign: α = 0.1, with circle: α =0.125, with asterisk: α =0.15, with cross: α =0.175, with square: α =0.2, with diamond: α =0.225, with triangle-downward: α =0.25, with triangle-upward: α =0.275, with triangle-right: α = 0.3.). The standard deviation data come from Figure 26.

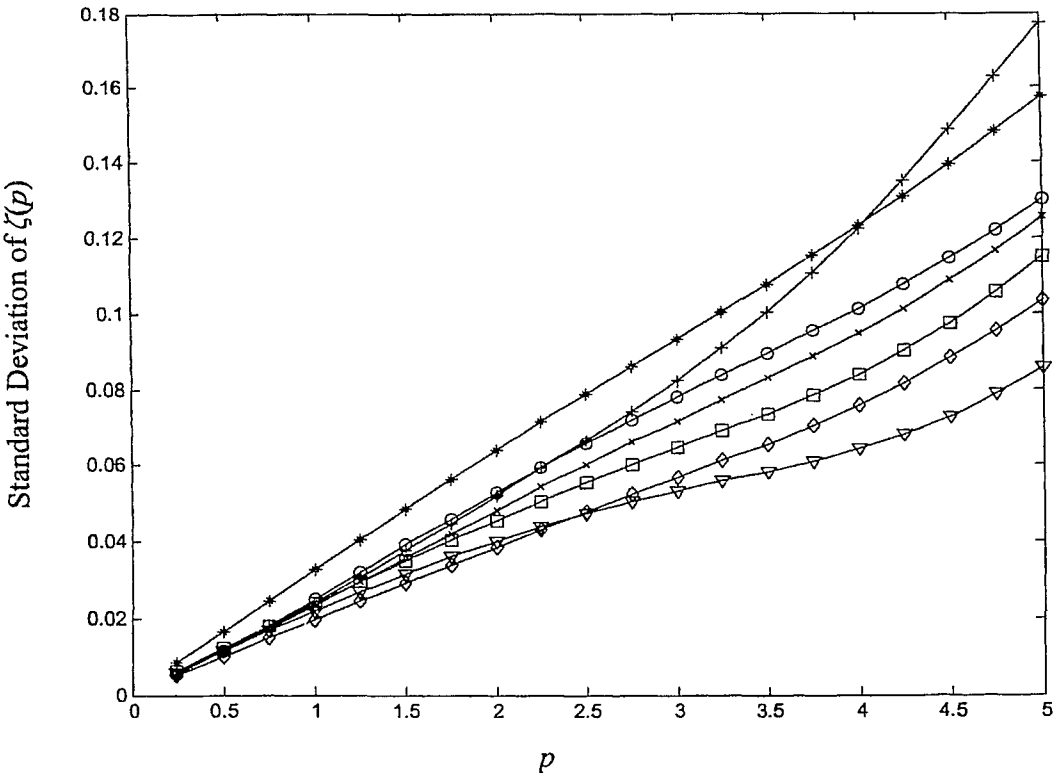

Figure 31. Standard deviation of $\zeta(p)$ versus p in μ group (Solid line with plus sign: μ = 0.4, with circle: μ =0.6, with asterisk: μ =0.8, with cross: μ = 1, with square: μ =1.2, with diamond: μ =1.4, with triangle-downward: μ =1.6.). The standard deviation data come from Figure 27.

4.2 Hierarchy

To prove the hierarchical structure in LFGC model, the same approach is followed in Section 2.2 by substituting the structure function of the LFGC generated $r_j(t)$ into (13) and (14): i.e., for a pair of fixed τ_1 and τ_2, consider

$$\left[\frac{S_{p+2}(\tau_1)}{S_{p+1}(\tau_1)}\right] = A_p\left[\frac{S_{p+1}(\tau_1)}{S_p(\tau_1)}\right]^{\beta} S^{\infty}(\tau_1)^{1-\beta} \tag{13}$$

$$\left[\frac{S_{p+2}(\tau_2)}{S_{p+1}(\tau_2)}\right] = A_p\left[\frac{S_{p+1}(\tau_2)}{S_p(\tau_2)}\right]^{\beta} S^{\infty}(\tau_2)^{1-\beta}. \tag{14}$$

Then the power law relationship (16) is checked to validate the hierarchy in the LFGC generated time series:

$$V_{\tau_1,\tau_2}(p+1) \sim V_{\tau_1,\tau_2}(p)^{\beta} \tag{16}$$

where $V_{\tau_1\tau_2}(p) = \left(S_{p+1}(\tau_2)/S_{p+1}(\tau_2)\right)/\left(S_p(\tau_1)/S_p(\tau_1)\right)$.

As p varies from 0.25 to 5, the power law behavior indeed was found when both sides of (16) are plotted on a log-log scale; see Figure 32 and Figure 33 for the typical case (V_f= 1, μ =1, α = 0.2). Also, τ_1 and τ_2 are varied to check the consistency of β estimate. Table 4 and Table 5 show the results of this calculation. The estimated β value is found to vary slightly with the τ_1 and τ_2 parameters, as it should be.

The β values of the α – and μ – group are summarized in Figures 34 and 35, respectively. In both cases, the estimates are made for $\tau_1 = 2^6$ and $\tau_2 = 2^{10}$. Figure 33 shows that β is an increasing function of α. This is consistent with the model (10) and the $\zeta(p)$ results in Section 4.1. For (10), it can be seen that, as β approaches 1, the corresponding $\zeta(p)$ becomes more linear. In the $\zeta(p)$ results, it was found the consistent result that a larger α implies a $\zeta(p)$ with less curvature. Figure 35 shows a similar rising trend between β and μ .

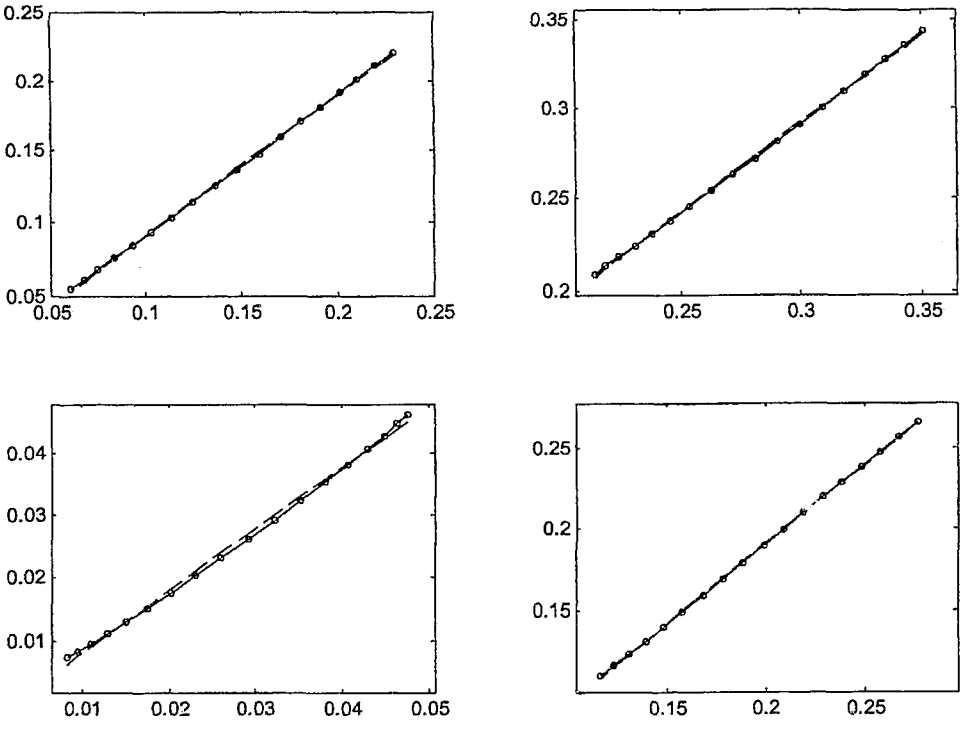

Figure 32. Hierarchy line in control case for LFGC model. In figure circles are data points, solid line is connecting line between data points and dash line is a fitting line. With p = 0.25 ~5 Abscissa: $\log_2(V_{\tau_1,\tau_2}(p))$;
Ordinate: $\log_2(V_{\tau_1,\tau_2}(p+1))$.

Table 4. Mean β values for different τ_1 and τ_2

$\tau_1=2^5,\tau_2=2^9,\beta=0.8467$	$\tau_1=2^3,\tau_2=2^9,\beta=0.9358$
$\tau_1=2^5,\tau_2=2^6,\beta=0.8344$	$\tau_1=2^4,\tau_2=2^{10},\beta=0.9151$

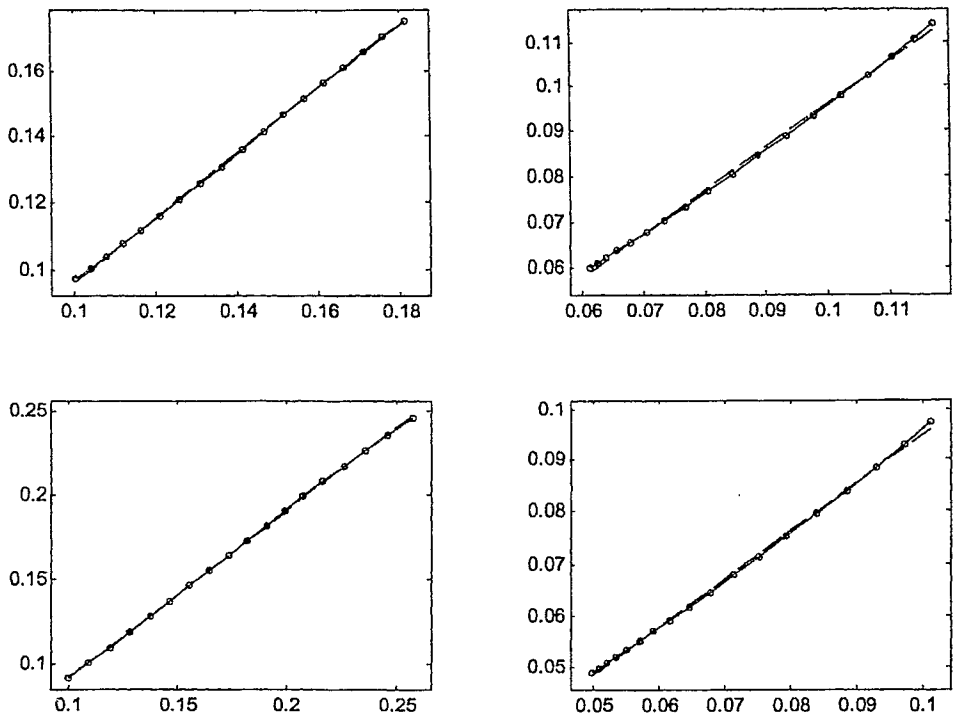

Figure 33. Hierarchy line in control case for LFGC model. In figure circles are data points, solid line is connecting line between data points and dash line is a fitting line. With p = 0.25 ~5 Abscissa: $\log_2(V_{\tau_1,\tau_2}(p))$;
Ordinate: $\log_2(V_{\tau_1,\tau_2}(p+1))$.

Table 5. mean β values for different τ_1 and τ_2

$\tau_1=2^3,\tau_2=2^6,\beta=0.8558$	$\tau_1=2^6,\tau_2=2^8,\beta=0.7875$
$\tau_1=2^5,\tau_2=2^{11},\beta=0.8525$	$\tau_1=2^7,\tau_2=2^{12},\beta=0.8088$

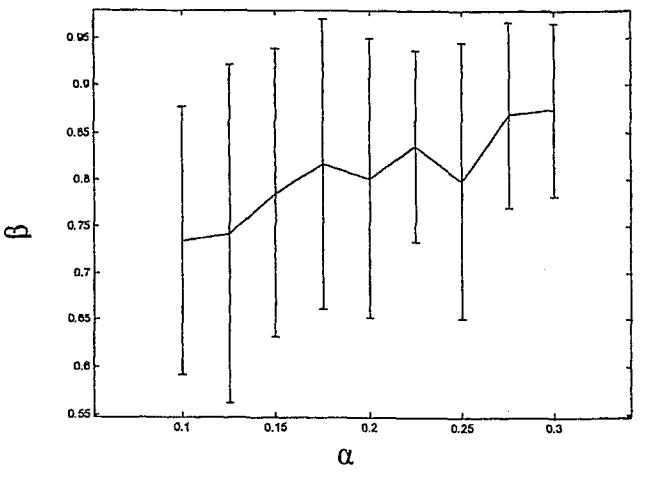

Figure 34. the β parameters for α group. Confidence interval for β is within its mean plus or minus one standard deviation.

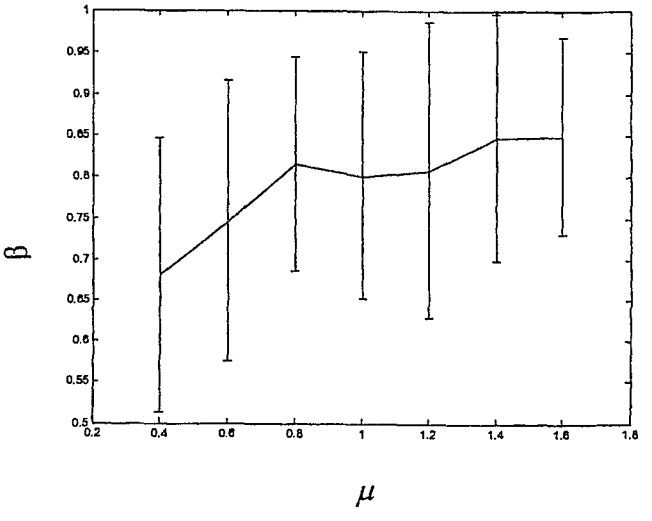

Figure 35. the β parameters for μ group. Confidence interval for β is within its mean plus or minus one standard deviation.

Chapter 5

Conclusion and Future Work

From the simulation results it can be concluded that the LFGC model can effectively capture the HRV phenomenology; including the 1/f power law, self-similarity, SEG transition of the increment PDF and multifractality. From the signal property point of view, this result implies a rather "stable" cascade-generated HRV phenomenology against "perturbation" by the feedback. In terms of the cardiovascular regulation, the numerical results suggest that feedback plays a less dominant role in the HRV genesis. It can be conjectured that the apparent random fluctuation of the heart rate is caused by the interaction of the higher control centers in the brain stem and the autonomic nervous system. This view is consistent with the recent study of the prolonged bad rest test [20]: it was found that the feedback-dominant baroreflex mechanism generates very different dynamics in the blood pressure fluctuation than the RRi dynamics.

The observation of the SL hierarchy in HRV provides the main motivation for the LFGC model. Although comparing the effect of the modulation effect in SW cascade with biological feedback and the scheduling law of the LFGC model are assumptions which cannot be easily verified in physiological terms, LFGC is interesting in its own right as it may represent a second solution to the SL hierarchy besides the SW cascade. However, more numerical tests are necessary to confirm this possibility [21].

The physiological implementation of the numerical results is not clear at this stage. More tests are needed for this purpose in the future. Also, only the parameters α and μ are varied. In this work, the influence of the parameter V_j to the underlying LFGC phenomenology remains to be tested in the future. It would also be interesting to test the outcomes of the model by perturbing the cascade, such as its tree structure, distribution of the cascade component, multiplicative law, as well as the feedback control with a different scheduling law.

Appendix A

Moments of Product of Cascade Components

The moment of the product of cascade components, which characterizes how the observable varies at different scales, has a relationship with the underlying scales. This can be most easily shown in the cascade generated by independent and identically distributed (i.i.d.) components. In fluid turbulence, such a multiplicative structure is normally used to characterize the dissipation and the primary variable of interest is the product of the cascade components (rather than the increment). In this case, the dependence of the statistics on scales can be found analytically.

Consider the cascade generated by i.i.d. components. The product of the cascade components observed at two scales l and l_n is given by

$$W_{l,l_n} = \prod_{m=l}^{L_n} \omega_m \tag{A.1}$$

where ω_m's are assumed i.i.d. Assuming dyadic cascade as in the present work and there are n-generation between scales l and l_n, then p^{th}-order moment of $|W_{l,l_n}|$ can be written in logarithmic scales

$$\log(\langle |W_{l,l_n}|^p \rangle) \sim n \log(\langle |\omega|^p \rangle) \tag{A.2}$$

where ω is the same random variable as the ω_m's. Note that for dyadic cascade, $l_n/l = 2^{-n}$. Substituting n, (A.2) becomes

$$\log_2\left(\left\langle |W_{l,l_n}|^p \right\rangle\right) \sim -\xi_n \log_2\left(\frac{l_n}{l}\right)$$

where $\xi_n = \log_2\left(\left\langle |\omega|^p \right\rangle\right)$. Hence, the product of i.i.d. random variables on regular dyadic cascade has its moment statistics dependent on the scales via a power law relationship.

For bounded cascade where the cascade components are not i.i.d., the formulation is more involved. When the primary statistic of interest is the moment of the increment, such as the structure function, numerical simulation indicated a similar scale dependence relationship [5]. However, no analytical result for the structure function has been worked out for the bounded cascade in the past.

Appendix B

Main programs in Matlab

1. LFGC model program

```
% Dynamic Cascade Model with Local Feedback

% (1) set program parameters

isave=1;
postprocess1=1;
postprocess2=0;
ntrial=input('enter ntrial:');

% (2) set cascade parameters

J=15;
N=32768;
delta=2^J./2.^(1:J);
J1=fix(log2(N));
k=ones(1,J)*1;

tau=2.^linspace(0,J-1,J);
ntau=J;
if J==J1,ntau1=ntau;else,ntau1=J1;end
q=.25:.25:5;
nq=length(q);

sig0=2^(-1.5);alpha=0.2;
sig00=sig0*2.^(-alpha*(0:J-1));

% (3) define set point Vj, mu & initialize w at t=0

V=ones(J,1);
mu=ones(J,1)*1.6;
w=zeros(J,N+1);
w(:,1)=randn(J,1).*sig00'+mu;

% (4) set control related parameters

buffer=abs(w(2:J,1)-V(2:J));

for itrial=1:ntrial
disp(num2str(itrial));

for i=2:N  % time=1~N corresponds to i=1~N
    wlast=w(:,i-1);
    pert_jp1=randn*sig00(J);
```

```
    w(J,i)=mu(J)+pert_jp1;
    skip=0;
    for j=J-1:-1:1
        if mod(i-1,delta(j))~=0
           w(j,i)=wlast(j);
           buffer(j)=buffer(j)+abs(wlast(j+1)-V(j+1)); %coupled from
smaller scale
        else
           w(j+1,i)=mu(j+1)+pert_jp1*(V(j)-buffer(j)/delta(j));
           %w(j+1,i)=mu(j+1);
           pert_jp1=randn*sig00(j);
           w(j,i)=mu(j)+pert_jp1;
           buffer(j)=abs(w(j+1,i)-V(j+1));
        end
    end

end
x=prod(w);
if isave,xs(itrial,:)=x;end

if postprocess1
for i=1:ntau1
    dx=x(1+tau(i):N)-x(1:N-tau(i));
    for j=1:nq
        s(itrial,j,i)=mean(abs(dx).^q(j));
    end
    [p(itrial,i,:),b(itrial,i,:)]=normhist(dx,41,min(dx),max(dx));
end
end
clear x
end
save 18v=1mu=1.6alpha=0.2.mat b p s xs

% system parameters:
% w [J-by-N+1]: the cascade components where
%     w(j,i) describes the jth level w value at time i
%     Note that time goes from 0 to N (N+1 samples).
% V [N-by-1]: the control level for w to return to.
% mu [N-by-1]: mean of w(j,:)
% sig0, alpha: the variance law of the bounded cascade
% buffer [(J-1)-by-1]: the control law to adjust the
%     w(j,:) to return to V at time t_k^{(j-1)}.
%
% NOTES:
%
% A Deviation btn. V and mu results in 'miss-targeted'
%   control and larger the deviation, more intermittent-
%   looking x(t).
```

2. Increment PDF program for typical real HRV

```
fn=input('enter filename:','s'); % file can be opened in workspace so
it is not needed eval(['load ' fn]);
N=length(x);
%J=fix(log2(N));
```

```
J=15;
tau=2.^linspace(0,J-1,J);
ntau=length(tau);
q=(0.25:.25:5);
nq=length(q);
for j=1:ntau
        dx=x(1+tau(j):N)-x(1:N-tau(j));

        % calculate structure function
        for k=1:nq
            s(k,j)=mean(abs(dx).^q(k));
        end
        % calculate distribution (pdf)
        b(j,:)=linspace(min(dx),max(dx),41);
        p(j,:)=hist(dx,b(j,:));
        p(j,:)=p(j,:)./sum(p(j,:)*(b(j,2)-b(j,1)));
    end

plot(2.2*b(1,:),(1/2.2).*log2(p(1,:)),'bo',2.2*b(1,:),(1/2.2).*log2(p(1
,:)),'b-')
   hold on

plot(1.5*b(5,:),(1/1.5).*log2(p(5,:)),'ro',1.5*b(5,:),(1/1.5).*log2(p(5
,:)),'r-')
   hold on

plot(1.2*b(9,:),(1/1.2).*log2(p(9,:)),'co',1.2*b(9,:),(1/1.2).*log2(p(9
,:)),'c-')
   hold on
   plot(b(12,:),log2(p(12,:)),'go',b(12,:),log2(p(12,:)),'g-')
   xlabel('f_{0}\Deltar')
   ylabel('log_{2}(f_{\tau}(\Deltar)/f_{0})')
   title('RRi increment PDF')%gtext('\tau')
```

3. Increment PDF program for LFGC model

```
% finding the pdf among the 100 run in different tau
fn=input('enter filename:','s');
eval(['load ' fn]);

for k=1
    ntau=k; % different tau
for i=1:100
    u(i)=max(b(i,ntau,:));  % u denotes up level of bin and 1 is NO. of
tau-can be changed
    d(i)=min(b(i,ntau,:));  % d denots down level of bin and 1 is NO.
of tau
end
umax=max(u);  % finding the minimun value of up level of bin
dmin=min(d);  % finding the maximun value of down level of bin
bk=linspace(dmin,umax,60); % seting up a new bin 30 is the reduced
value for 41
for i=1:100
    br(i,:)=b(i,ntau,:);  % reducing the dimension of matrix due to
Matlab limitation
```

```
    pr(i,:)=p(i,ntau,:);   % same reason  1 is No. of tau- can be
replaced

        t(i,:)=interp1(br(i,:),log2(pr(i,:)),bk);

end
% tm=mean(t);
for i=1:60
    m(i)=0;
    sum(i)=0;
    for j=1:100
        sum(i)=sum(i)+t(j,i);
        if t(j,i)==0
            m(i)=m(i)+1
        end
    end

end
for i=1:60
    tm(i)=sum(i)/(100-m(i));
end
plot(bk,tm,'b+',bk,tm,'g-')
hold on
%save case1 bk t
clear u d umin dmax
end
for k=4
    ntau=k; % different tau
for i=1:100
    u(i)=max(b(i,ntau,:));  % u denotes up level of bin and 1 is NO. of
tau-can be changed
    d(i)=min(b(i,ntau,:));  % d denots down level of bin and 1 is NO.
of tau
end
umax=max(u);  % finding the minimun value of up level of bin
dmin=min(d);  % finding the maximun value of down level of bin
bk=linspace(dmin,umax,60); % seting up a new bin 30 is the reduced
value for 41
for i=1:100
    br(i,:)=b(i,ntau,:);  % reducing the dimension of matrix due to
Matlab limitation
    pr(i,:)=p(i,ntau,:);   % same reason  1 is No. of tau- can be
replaced

        t(i,:)=interp1(br(i,:),log2(pr(i,:)),bk);

end
% tm=mean(t);
for i=1:60
    m(i)=0;
    sum(i)=0;
    for j=1:100
        sum(i)=sum(i)+t(j,i);
        if t(j,i)==0
            m(i)=m(i)+1
        end
    end
```

```
end
for i=1:60
    tm(i)=sum(i)/(100-m(i));
end
plot(bk,tm,'b+',bk,tm,'c-')
hold on
%save case1 bk t
clear u d umin dmax
end
for k=8
    ntau=k; % different tau
for i=1:100
    u(i)=max(b(i,ntau,:));  % u denotes up level of bin and 1 is NO. of
tau-can be changed
    d(i)=min(b(i,ntau,:));  % d denots down level of bin and 1 is NO.
of tau
end
umax=max(u);  % finding the minimun value of up level of bin
dmin=min(d);  % finding the maximun value of down level of bin
bk=linspace(dmin,umax,60); % seting up a new bin 30 is the reduced
value for 41
for i=1:100
    br(i,:)=b(i,ntau,:);  % reducing the dimension of matrix due to
Matlab limitation
    pr(i,:)=p(i,ntau,:);   % same reason  1 is No. of tau- can be
replaced

        t(i,:)=interp1(br(i,:),log2(pr(i,:)),bk);

end
% tm=mean(t);
for i=1:60
    m(i)=0;
    sum(i)=0;
    for j=1:100
        sum(i)=sum(i)+t(j,i);
        if t(j,i)==0
            m(i)=m(i)+1
        end
    end
end
for i=1:60
    tm(i)=sum(i)/(100-m(i));
end
plot(bk,tm,'bx',bk,tm,'m-')
hold on
%save case1 bk t
clear u d umin dmax
end
for k=12
    ntau=k; % different tau
for i=1:100
    u(i)=max(b(i,ntau,:));  % u denotes up level of bin and 1 is NO. of
tau-can be changed
    d(i)=min(b(i,ntau,:));  % d denots down level of bin and 1 is NO.
of tau
end
```

```
umax=max(u);  % finding the minimun value of up level of bin
dmin=min(d);  % finding the maximun value of down level of bin
bk=linspace(dmin,umax,60); % seting up a new bin 30 is the reduced
value for 41
for i=1:100
    br(i,:)=b(i,ntau,:);  % reducing the dimension of matrix due to
Matlab limitation
    pr(i,:)=p(i,ntau,:);   % same reason  1 is No. of tau- can be
replaced

        t(i,:)=interp1(br(i,:),log2(pr(i,:)),bk);

end
% tm=mean(t);
for i=1:60
    m(i)=0;
    sum(i)=0;
    for j=1:100
        sum(i)=sum(i)+t(j,i);
        if t(j,i)==0
            m(i)=m(i)+1
        end
    end
end
for i=1:60
    tm(i)=sum(i)/(100-m(i));
end
plot(bk,tm,'b+',bk,tm,'k-')
hold on
%save case1 bk t
clear u d umin dmax
end

for k=15
    ntau=k; % different tau
for i=1:100
    u(i)=max(b(i,ntau,:));  % u denotes up level of bin and 1 is NO. of
tau-can be changed
    d(i)=min(b(i,ntau,:));  % d denots down level of bin and 1 is NO.
of tau
end
umax=max(u);  % finding the minimun value of up level of bin
dmin=min(d);  % finding the maximun value of down level of bin
bk=linspace(dmin,umax,60); % seting up a new bin 30 is the reduced
value for 41
for i=1:100
    br(i,:)=b(i,ntau,:);  % reducing the dimension of matrix due to
Matlab limitation
    pr(i,:)=p(i,ntau,:);   % same reason  1 is No. of tau- can be
replaced

        t(i,:)=interp1(br(i,:),log2(pr(i,:)),bk);

end
% tm=mean(t);
for i=1:60
    m(i)=0;
```

```
    sum(i)=0;
    for j=1:100
        sum(i)=sum(i)+t(j,i);
        if t(j,i)==0
            m(i)=m(i)+1
        end
    end
end
for i=1:60
    tm(i)=sum(i)/(100-m(i));
end
plot(bk,tm,'bo',bk,tm,'r-')
hold on
%save case1 bk t
clear u d umin dmax
end

xlabel('\Deltar')
    ylabel('log_{2}(f_{\tau}(\Deltar))')
    title('Increment PDF for  v = 1 \mu = 1 \alpha = 0.2')
    %gtext('\tau = 2^0, 2^3, 2^7, 2^{11}, 2^{14}')
```

4. Kurtosis Curve program for typical real HRV

```
fn=input('enter filename:','s');
eval(['load ' fn]);
N=length(x);
%J=fix(log2(N));
J=15;
tau=2.^linspace(0,J-1,J);
ntau=length(tau);
q=(0.25:.25:5);
nq=length(q);

for itau=1
    dx1=x(1+tau(itau):N)-x(1:N-tau(itau));
   ku(itau)=kurtosis(dx1);
end
for itau=2
    dx2=x(1+tau(itau):N)-x(1:N-tau(itau));
   ku(itau)=kurtosis(dx2);
end
for itau=3
    dx3=x(1+tau(itau):N)-x(1:N-tau(itau));
   ku(itau)=kurtosis(dx3);
end
for itau=4
    dx4=x(1+tau(itau):N)-x(1:N-tau(itau));
   ku(itau)=kurtosis(dx4);
end
for itau=5
    dx5=x(1+tau(itau):N)-x(1:N-tau(itau));
   ku(itau)=kurtosis(dx5);
end
for itau=6
```

```
    dx6=x(1+tau(itau):N)-x(1:N-tau(itau));
   ku(itau)=kurtosis(dx6);
end
for itau=7
    dx7=x(1+tau(itau):N)-x(1:N-tau(itau));
   ku(itau)=kurtosis(dx7);
end
for itau=8
    dx8=x(1+tau(itau):N)-x(1:N-tau(itau));
   ku(itau)=kurtosis(dx8);
end
for itau=9
    dx9=x(1+tau(itau):N)-x(1:N-tau(itau));
   ku(itau)=kurtosis(dx9);
end
for itau=10
    dx10=x(1+tau(itau):N)-x(1:N-tau(itau));
   ku(itau)=kurtosis(dx10);
end
for itau=11
    dx11=x(1+tau(itau):N)-x(1:N-tau(itau));
   ku(itau)=kurtosis(dx11);
end
for itau=12
    dx12=x(1+tau(itau):N)-x(1:N-tau(itau));
   ku(itau)=kurtosis(dx12);
end
for itau=13
    dx13=x(1+tau(itau):N)-x(1:N-tau(itau));
   ku(itau)=kurtosis(dx13);
end
for itau=14
    dx14=x(1+tau(itau):N)-x(1:N-tau(itau));
   ku(itau)=kurtosis(dx14);
end
for itau=15
    dx15=x(1+tau(itau):N)-x(1:N-tau(itau));
   ku(itau)=kurtosis(dx15);
end
plot(log2(tau),log2(ku),'bo')
hold on
plot(log2(tau),log2(ku),'g-')
hold on
%line=polyfit(log2(tau),log2(ku),1);
%z=polyval(line,log2(tau));
%plot(log2(tau),z,'r--')
grid on;
    [scrnx,scrny]=ginput(2);
    id1=min(find(log2(tau) >= scrnx(1)));
    id2=max(find(log2(tau) <= scrnx(2)));
    c=polyfit(log2(tau(id1:id2)),log2(ku(id1:id2)),1);
    rzeta2=c(1);
grid off;
z=polyval(c,log2(tau));
plot(log2(tau),z,'r--')
xlabel('log_2(\tau)')
ylabel('log_2(Kurtosis)')
```

```
title(' Real HRV Kurtosis Curve2')
```

5. Kurtosis Curve program for LFGC model

```
% Based on 100 simulation
fn=input('enter filename:','s'); % file can be opened in workspace so
it is not needed for me
eval(['load ' fn]);
N=32768;
J=15;
tau=2.^linspace(0,J-1,J);
ntau=length(tau);
q=(0.25:.25:5);
nq=length(q);
for i=1:100
    x=xs(i,:);
   for itau=1
    dx1=x(1+tau(itau):N)-x(1:N-tau(itau));
   ku(i,itau)=kurtosis(dx1);
   clear dx1
end
for itau=2
    dx2=x(1+tau(itau):N)-x(1:N-tau(itau));
   ku(i,itau)=kurtosis(dx2);
   clear dx2
end
for itau=3
    dx3=x(1+tau(itau):N)-x(1:N-tau(itau));
   ku(i,itau)=kurtosis(dx3);
   clear dx3
end
for itau=4
    dx4=x(1+tau(itau):N)-x(1:N-tau(itau));
   ku(i,itau)=kurtosis(dx4);
   clear dx4
end
for itau=5
    dx5=x(1+tau(itau):N)-x(1:N-tau(itau));
   ku(i,itau)=kurtosis(dx5);
   clear dx5
end
for itau=6
    dx6=x(1+tau(itau):N)-x(1:N-tau(itau));
   ku(i,itau)=kurtosis(dx6);
   clear dx6
end
for itau=7
    dx7=x(1+tau(itau):N)-x(1:N-tau(itau));
   ku(i,itau)=kurtosis(dx7);
   clear dx7
end
for itau=8
    dx8=x(1+tau(itau):N)-x(1:N-tau(itau));
   ku(i,itau)=kurtosis(dx8);
   clear dx8
```

```
end
for itau=9
    dx9=x(1+tau(itau):N)-x(1:N-tau(itau));
   ku(i,itau)=kurtosis(dx9);
   clear dx
end
for itau=10
    dx10=x(1+tau(itau):N)-x(1:N-tau(itau));
   ku(i,itau)=kurtosis(dx10);
   clear dx
end
for itau=11
    dx11=x(1+tau(itau):N)-x(1:N-tau(itau));
   ku(i,itau)=kurtosis(dx11);
   clear dx11
end
for itau=12
    dx12=x(1+tau(itau):N)-x(1:N-tau(itau));
   ku(i,itau)=kurtosis(dx12);
   clear dx12
end
for itau=13
    dx13=x(1+tau(itau):N)-x(1:N-tau(itau));
   ku(i,itau)=kurtosis(dx13);
   clear dx13
end
for ' au=14
    dx14=x(1+tau(itau):N)-x(1:N-tau(itau));
   ku(i,itau)=kurtosis(dx14);
   clear dx14
end
for itau=15
    dx15=x(1+tau(itau):N)-x(1:N-tau(itau));
   ku(i,itau)=kurtosis(dx15);
   clear dx15
end
clear x
end
kur=mean(ku);
plot(log2(tau),log2(kur),'bo')
hold on
plot(log2(tau),log2(kur),'g-')
hold on
grid on;
[scrnx,scrny]=ginput(2);
id1=min(find(log2(tau) >= scrnx(1)));
id2=max(find(log2(tau) <= scrnx(2)));
c=polyfit(log2(tau(id1:id2)),log2(kur(id1:id2)),1);
z5(i)=c(1);
grid off;
z=polyval(c,log2(tau));
plot(log2(tau),z,'r--')
 xlabel('log_2(\tau)')
 ylabel('log_2(Kurtosis)')
 title('Kurtosis Curve for  V = 1 \mu = 0.1 \alpha = 0.2')
```

6. Hierarchical structure program for typical HRV

```
fn=input('enter filename:','s');
eval(['load ' fn]);
N=length(x);
%J=fix(log2(N));
J=15;
tau=2.^linspace(0,J-1,J);
ntau=length(tau);
q=(0.25:.25:5);
nq=length(q);

for j=1:ntau
        dx=x(1+tau(j):N)-x(1:N-tau(j));

        % calculate structure function
        for k=1:nq
            s(k,j)=mean(abs(dx).^q(k));
        end

    end
tau1=7;
tau2=11;

q=20;
sh1(1:q)=s(1:q,tau1);
a1(1:18)=sh1(3:20)./sh1(2:19);
b1(1:18)=sh1(2:19)./sh1(1:18);
sh2(1:q)=s(1:q,tau2);
a2(1:18)=sh2(3:20)./sh2(2:19);
b2(1:18)=sh2(2:19)./sh2(1:18);
a(1:18)=a2(1:18)./a1(1:18);
b(1:18)=b2(1:18)./b1(1:18);
clear tau1 tau2 q sh1 sh2 a1 b1 a2 b2
plot(log2(b(1:18)),log2(a(1:18)),'bo')
hold on
plot(log2(b(1:18)),log2(a(1:18)),'k-')
hold on

c=polyfit(log2(b(1:18)),log2(a(1:18)),1);
typical_hrv=c(1)^4;

 z=polyval(c,log2(b(1:18)));
plot(log2(b(1:18)),z,'r--')
title('Hierachical Structure Line in Typical HRV')
gtext('\tau_1=2^6, \tau_2=2^{10}')
legend('datum point','connecting line','fitting line')
```

7. Hierarchical structure program for LFGC model

```
    ( Program after % can be used for one trial plotting)
% Hirarchy structure test
fn=input('enter filename:','s');
```

```
eval(['load ' fn]);
tau1=7; % control case V=1 mu=1 alpha=0.2
tau2=11;
for itrial=1:100
q=20;
sh1(itrial,1:q)=s(itrial,1:q,tau1);
a1(itrial,1:18)=sh1(itrial,3:20)./sh1(itrial,2:19);
b1(itrial,1:18)=sh1(itrial,2:19)./sh1(itrial,1:18);
sh2(itrial,1:q)=s(itrial,1:q,tau2);
a2(itrial,1:18)=sh2(itrial,3:20)./sh2(itrial,2:19);
b2(itrial,1:18)=sh2(itrial,2:19)./sh2(itrial,1:18);
a(itrial,1:18)=a2(itrial,1:18)./a1(itrial,1:18);
b(itrial,1:18)=b2(itrial,1:18)./b1(itrial,1:18);
% clear tau1 tau2 q sh1 sh2 a1 b1 a2 b2
% plot(log2(b(itrial,1:18)),log2(a(itrial,1:18)),'bo')
% hold on
% plot(log2(b(itrial,1:18)),log2(a(itrial,1:18)),'g-')
% hold on

c=polyfit(log2(b(itrial,1:18)),log2(a(itrial,1:18)),1);
shcase18(itrial)=c(1)^4;
end
clear tau1 tau2 q sh1 sh2 a1 b1 a2 b2
% z=polyval(c,log2(b(itrial,1:18)));
% plot(log2(b(itrial,1:18)),z,'r--')
% legend('datum point','Hierachical line','Linear-fitted line')
% xlabel('log_2 Hx')
% ylabel('log_2 Hy')
% title('Hierachical Structure Line in simulatin 100 for control case')
clear a b c itrial z
shcase18m=mean(shcase18);
plot(shcase18,'bo')
hold on
plot(shcase18,'g-')
hold on
y(1:101)=shcase18m;
x=0:100;
plot(x,y,'r-')
xlabel('No. of Simulation')
ylabel('\beta')
title('\beta value in case V =1 \mu =1.6 \alpha = 0.2')
legend('datum point','connecting line','average \beta value')
save beta18 shcase18
```

8. Program for finding slope of structure function

```
find zeta
fn=input('enter filename:','s');
eval(['load ' fn]);
[ncases,nq,ntau]=size(s);
for i=1:ncases
    ss=squeeze(s(i,:,:));
    plot(log2(ss(12,:)),'o-');
    grid on;
    [scrnx,scrny]=ginput(2);
```

```
    id=ceil(scrnx(1)):1:fix(scrnx(2));
    for iq=1:nq
        cc=polyfit(id,log2(ss(iq,id)),1);
        zeta9(i,iq)=cc(1);
  end
end
```

Reference:

[1] M.Kobayashi and T. Musha, *1/f Fluctuation of heartbeat period,* IEEE. transaction. Biomed. Engng. 29:456-457(1982).

[2] Y. Nakamura, Y. Yamamoto, and I. Muraoka, *Autonomic control of heart rate during physical exercise and fractal dimension of heart rate variability,* J. Appl. Physiol. 74: 875-881(1993).

[3] J. T. Bigger Jr, R. C. Steinman, L. M. Rolnitzky, J. L. Fleiss, P. Albrecht and R. J. Cohen, *Power law behavior of RR-interval variability in healthy middle-aged persons, patients with recent acute myocardial infarction, and patients with heart transplants,* Circulation. 93: 2142-51(1996).

[4] B.J. West, R. Zhang, A.W. Sanders, S. Miniyar, J.H. Zuckerman and B.D. Levine, *Fractal fluctuations in cardiac time series,* Physica A, 270: 552-566(1999).

[5] D.C Lin and R.L. Hughson, *A Phenomenology Model of normal sinus rhythm in healthy humans,* IEEE. transaction. Biomed. Engng. 49:97-109(2002).

[6] R. Benzi and L. Biferale, *Multifractality in the statistics of the velocity gradients in turbulence,* Phys. Rev. Lett. 67:2299–2302 (1991).

[7] D. C. Lin and R. L. Hughson, *Using Gaussians to model increment distribution of the long-term R-wave interval in healthy humans,* Chaos, Solitons & Fractals12: 1335-1345(2001).

[8] J. J. A. Moors, *The Meaning of Kurtosis: Darlington Reexamined,* Amer. Statist. 40: 283-284(1986).

[9] P. J. Bickel and E. L. Lehmann, *Descriptive statistics for nonparametric models.* I *Introduction,* The annals of Statistics 3: 1038-1044 (1975).

[10] D. Rupert, *What is Kurtosis? An Influence Function Approach,* Amer. Statist. 41: 1-5(1987).

[11] N. L. Johnson and S. Kotz, *Encyclopedia of statistical science* (Vol. 5), New York, John Wiley (1985).

[12] D.C. Lin and R.L. Hughson, *Modeling heart rate variability in healthy humans: a turbulence analogy,* Phys. Rev. Lett. 86: 1650-1653(2001).

[13] P. Ch. Ivanov, L. A. Nunes, Amaral, A. L. Goldberger and H. E. Stanley, *Stochastic feedback and the regulation of biological rhythms,* Europhys. Lett. 43:363-368 (1998).

[14] D. Lin, *Robustness and perturbation in the modeled cascade heart rate variability,* Phys. Rev. E. 67:1914-1921 (2003).

[15] W. Feller, *Introduction to Probability and Its applications, Vol.* 2, John wiley & sons, New York.(1971).

[16] Robert C. Little, William C. Little, *Physiology of the Heart and circulation,* Fourth Edition, Year Book Medical Publishers, Chicago IL, (1989).

[17] Zhen-Su She and Edward C. Waymire, *Quantized Energy Cascade and Log-Poisson Statistics in Fully Developed Turbulence,* Phys. Rev. Lett. 74: 262–265(1994)

[18] Zhen-Su She and Emmanuel Leveque, *Universal Scaling Laws in Fully developed Turbulence,* Phys. Rev. Lett. 72: 336-339(1994).

[19] *Using MATLAB version 6,* The Mathworks Incorporated.

[20] J. O. Fortrat, D. Sigaudo, R. L. Hughson, A. Maillet, Y. Yamamoto, and C. Gharib, *Effect of prolonged head-down bed rest on complex cardiovascular dynamics,* Autonomic Neuroscience 86: 192-201 (2001).

[21]X.Z. Gao, E.S.C. Ching and D.C. Lin, *Hierarchical Structure of Heart Rate Variability in Humans,* Symposium of Physics in Physiology, Annual APS March Meeting 2004, Montreal.